The ExB staircase of magnetised plasmas

Guilhem Dif-Pradalier, G. Hornung, X. Garbet, Ph. Ghendrih, V. Grandgirard, G. Latu, Y. Sarazin

The **E** × **B** staircase of magnetised plasmas

2017 Nucl. Fusion 57 066026

(http://iopscience.iop.org/0029-5515/57/6/066026)

IOP Publishing | International Atomic Energy Agency Nuclear Fusion

Nucl. Fusion **57** (2017) 066026 (20pp) https://doi.org/10.1088/1741-4326/aa6873

The $\mathbf{E} \times \mathbf{B}$ staircase of magnetised plasmas

G. Dif-Pradalier[1], G. Hornung[2], X. Garbet[1], Ph. Ghendrih[1], V. Grandgirard[1], G. Latu[1] and Y. Sarazin[1]

[1] CEA, IRFM, F-13108 St. Paul-lez-Durance cedex, France
[2] Department of Applied Physics, Ghent University, 9000 Gent, Belgium

E-mail: guilhem.dif-pradalier@cea.fr

Received 15 December 2016, revised 14 March 2017
Accepted for publication 22 March 2017
Published 26 April 2017

Abstract

We show that a class of near-marginal and low-collisional magnetised plasmas naturally evolve into a globally organised state dubbed the '$\mathbf{E} \times \mathbf{B}$ staircase'. A key signature of this self-organised state is the containment of avalanche activity, detrimental for confinement, by a series of microbarriers for transport, the staircase steps, beneficial for confinement. Conditions for existence of the $\mathbf{E} \times \mathbf{B}$ staircase, impact on transport and confinement and robustness in parameter space are discussed.

Keywords: turbulence, self-organisation, magnetised plasma

(Some figures may appear in colour only in the online journal)

We show that out-of-equilibrium magnetically confined near-marginal plasmas tend to naturally evolve towards a globally-organised critical state of spatially segregated microbarriers for transport and sectors of strong avalanche-like transport. We call this global pattern of avalanching sectors interspersed with narrow confining microbarriers the $\mathbf{E} \times \mathbf{B}$ *staircase* [1]. The present paper is concerned with discussing the factors that control this spatial segregation, the dynamics of this global organisation as well as its incidence on confinement.

The regime of near-marginality [2] is not merely academically-appealing for its rich dynamics and manifestations of self-organisation. It is as well a likely operating regime for current and future magnetic confinement devices. Non-burning ITER plasmas for instance, characterised by a large ratio of plasma volume over external heating are likely to reside close to marginal stability.

Relaxation through emission of fronts or avalanches [3–8] and turbulence regulation through zonal flow formation [9, 10] are natural trends of near-marginal drift-wave turbulence. One of the merits of $\mathbf{E} \times \mathbf{B}$ staircase patterning is certainly to provide, whilst segregating regions where avalanching is dominant from regions where zonal flow concentrates (forming the staircase microbarriers) a natural and dynamic means for both antagonistic trends to simultaneously exist.

Salient features of the $\mathbf{E} \times \mathbf{B}$ staircase are represented in figures 1 and 2 and summarised below:

(i) Ubiquitous signatures of staircase formation are mean profile corrugations, reflecting the propensity of an initially homogeneous near-marginal profile in a bath of drift-wave (or Rossby wave) turbulence to develop inhomogeneities that will tend to self-sharpen and endure. Self-sharpening relies upon positive feedback and may occur e.g. through negative viscosity-like arguments [11–14], clustering instability [15–17] or electric field curvature [18]. Which mechanism is operative in what region of parameter space is still unclear and will be focused on elsewhere. The *mean pressure profile corrugations* lead to strong localised temperature gradients (the 'risers' in figure 1). The name staircase comes from the step-like idealised resulting pressure profile with, *statistically*, quasi-constant mesoscale step spacing Δ. Corrugations are shown in figure 2 on the mean ion temperature gradient ∇T temporally-averaged over 0.53 ms between $1030\, a/c_s$ and $1343\, a/c_s$. The step size Δ is discussed below, item (v);

(ii) Co-located with the mean profile corrugations are zonal mean flows (section 2.2) or vorticity jumps that define lasting (from a few collision times to [at least] fractions of the energy confinement time) 'valleys' in configuration-time space of hindered transport. These zonal mean flows, of typical radial extent $\delta^{\mathrm{flow}} \sim 10\, \rho_s$ act as *a set of weak or permeable transport barriers* [19–21] that *regulate the turbulent heat flux* (section 2.3). They are thus also referred to as 'microbarriers' throughout the paper and are visible in figure 2 as coherent flux-

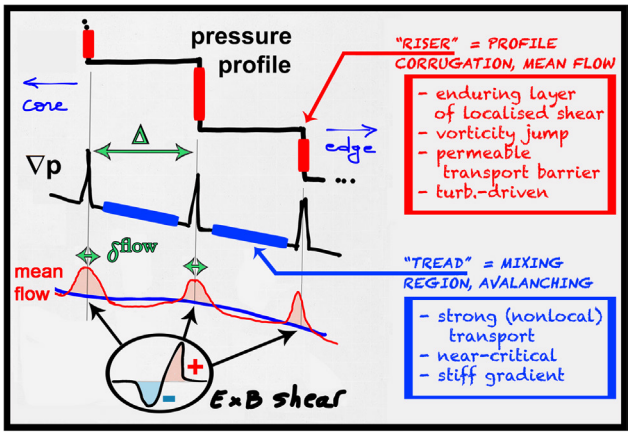

Figure 1. The $\mathbf{E}\times\mathbf{B}$ staircase, schematic view.

surface averaged $\mathbf{E}\times\mathbf{B}$ shear $\gamma_{\mathbf{E}\times\mathbf{B}} = r\partial_r(E_r/rB)$. The flux-surface averaged poloidal $\langle v_r v_\theta\rangle$ and toroidal $\langle v_r v_\varphi\rangle$ Reynolds stresses, the parallel momentum flux $\mathcal{M}_\parallel$ and the poloidal v_θ and toroidal flows v_φ similarly display long-lived structuring close to the mean profile corrugations. Regarding poloidal rotation, the *turbulence-borne* temperature corrugations at the staircase steps *neoclassically drive* [22] localised poloidal rotation $\propto \nabla T$ there, an example of synergistic interplay between collisions and turbulence [23];

(iii) The $\mathbf{E}\times\mathbf{B}$ staircase is a *near-marginal pattern* that progressively weakens and disappears with increasing distance to instability threshold (section 1.1);

(iv) The $\mathbf{E}\times\mathbf{B}$ staircase is a *weakly collisional pattern*, as expected from the fact that its microbarriers are zonal mean flows, hence sensitive to collisional damping [24] (section 1.2);

(v) Avalanches, in low to moderately heat-driven plasmas are ubiquitous. They play an important role for staircase dynamics given the near-marginal character of the latter. Avalanching is the dominant transport mechanism in-between the staircase shear layers (the 'treads' in figure 1), see item (vi) below. Avalanches, importantly, are statistically *contained by the staircase steps* (section 2.4.1) and rarely propagate across successive staircase shear layers and over a significant fraction of the plasma volume. The size distribution of avalanches therefore closely follows the size distribution of Δ (the 'tread width' or 'step size'). The most probable step size $\Delta^{\rm stat}\sim 40\,\rho_s$ is *mesoscale* (section 2.4.2), implying a *favourable mesoscale* (and not a macro-scale) *most probable scale length for avalanches*. Interestingly, despite strongly non-Gaussian statistics the *staircase mesoscale* $\Delta^{\rm stat}$ *reintroduces a favourable gyro-Bohm like scaling* for heat confinement (section 2.4);

(vi) Due to the avalanche activity, mixing in the 'treads' is strong. *Profiles there are stiff and transport is nonlocal and non-diffusive*, best described by a Lévy or a Lorentzian transport kernel of width Δ [1]. In the regions of the 'risers', heat transport is dominantly neoclassical [20], emphasising the fact that these regions are microbarriers for transport. $\Delta^{\rm stat}\sim 40\,\rho_s$ is a natural 'nonlocal' scale for the system, in addition to the 'local' autocorrelation microscale of the turbulence $\ell_c\sim 5-8\,\rho_s$. These two micro- and mesoscales, shown in figure 3 echo the two-scale turbulence correlation length [25] recently measured in Asdex-Upgrade. The measured mesoscale is a possible experimental characterisation of avalanche-staircase interplay;

(vii) The *flux-gradient relation is often multivalued and non-monotonic* near marginal stability, in contrast to oft-reported results in Ion Temperature Gradient turbulence [26]. In particular local values of the fluxes may not bijectively relate to local values of the gradients as different gradient drives may be associated to the same flux (multivalued) and larger gradient drives may be associated to lower fluxes (non-monotonic). Observation of coherent structures, as discussed here for the $\mathbf{E}\times\mathbf{B}$ staircase is often indication of a breakdown of the local

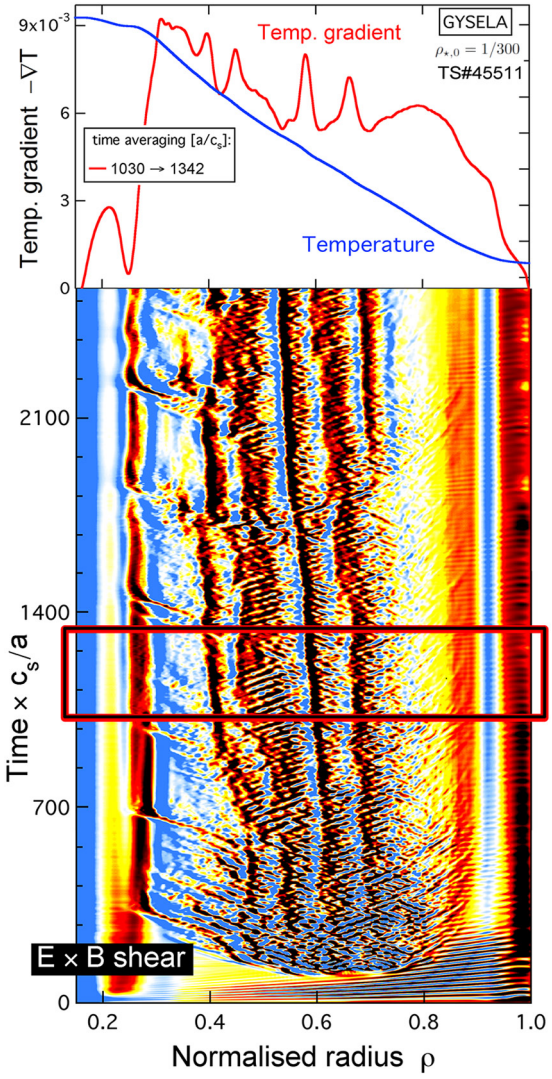

Figure 2. Three general features of the plasma staircase are visible here: (i) the mean profile corrugations here displayed on the temperature gradient, (ii) the strong, long-lived and coherent shear flows defining 'valleys' of hindered transport—the mean radial $\mathbf{E}\times\mathbf{B}$ shear profile is shown in figure 11 (left) and (iii) the radial transport dominated by avalanche-like events in-between the staircase steps.

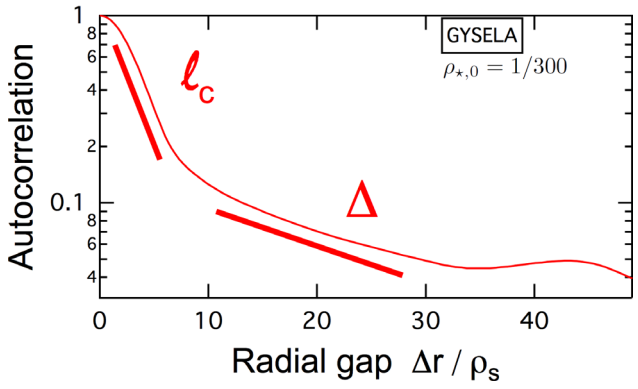

Figure 3. Autocorrelation of the electrostatic potential. Two slopes are found: the local autocorrelation length $\ell_c \sim 6\,\rho_s$ is microscale, the mesoscale is indicative of avalanches and therefore noted Δ (see section 2.4.1).

flux-gradient paradigm. This point is evoked in section 2.3 and will be further discussed elsewhere;

(viii) The whole *staircase pattern dynamically evolves and meanders*, river-like over intermediate to long (collisional to confinement) timescales as the staircase steps show propensity to remain at constant ambient gradient drive (section 3.2);

(ix) Where staircase steps (risers) nucleate does not rely upon special values of low-order safety factor q rationals, yet synergistic reinforcement of shear layers, as they meander, in proximity of a low-order q rational is sometimes observed (section 3.1). Passing electron dynamics may also modify turbulence organisation near low-order q rationals [27]. This is left for future work.

The results in this paper highlight robust properties of the $\mathbf{E}\times\mathbf{B}$ staircase and their impact on transport in L-mode-like plasmas. The discussion is based upon tens of gyrokinetic calculations representative of varying plasma parameters in drift-wave ion temperature gradient (ITG) turbulence with Boltzmann electrons, using the GYSELA code [28, 29]. Different main ion species are considered: Hydrogen, Deuterium or Helium, different collisionalities $\nu_\star = 0$ and $\nu_{\star,0} \in [0.005, 10]$, different plasma sizes $\rho_{\star,0}^{-1} \in [128, 512]$, different gradient drives $R/L_T \in [2, 12]$ or $\eta = L_n/L_T \in [1, 6]$, different heating mechanisms: thermal baths, gradient-driven and flux-driven and different boundary conditions. The subscript 0 stands for initial evaluation at mid-radius.

The main caveat of the present study lies in the assumption of a Boltzmann electron response which may impact turbulence organisation, especially in the vicinity of rational q surfaces [27]. Realistic flux-driven computations including both kinetic ion and electron responses are required to assess the generic character of staircase organisation, especially as ion and electron channels may interplay [21]. Such computations are unfortunately beyond reach of today's capabilities. A confidence-building step in the direction discussed throughout the paper comes from the robust observation of such patterns in varieties of *experimental* plasma conditions [20, 21].

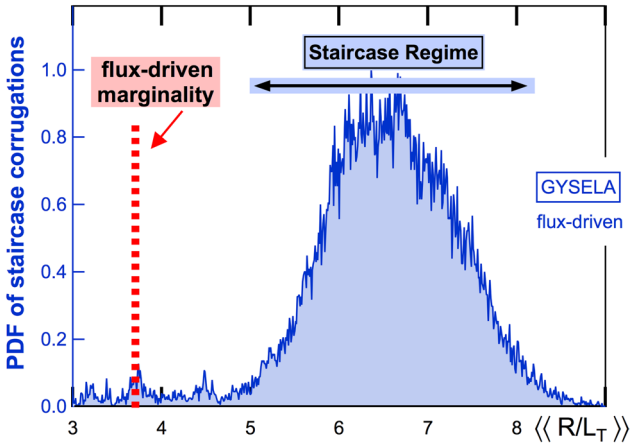

Figure 4. Where the $\mathbf{E}\times\mathbf{B}$ staircase exists as a function of the flux-driven normalised gradient drive $\langle\langle R/L_T\rangle\rangle$. Marginality for these parameters is indicated.

1. Staircases in parameter space: near-marginal and low-collisional

Whilst exploring plasma parameters, distance to instability threshold (distance to marginality) and collisionality stand out as key for $\mathbf{E}\times\mathbf{B}$ staircase organisation.

1.1. A near-marginal pattern

Temperature profile corrugations are ubiquitous staircase signatures. It is possible to systematically track in time the location $r_{\rm step}$ of these corrugations. These locations are themselves function of the thermodynamic gradients: $r_{\rm step}(L_T, L_n)$. Figure 4 represents the PDF of staircase corrugations as a function of $\langle\langle R/L_T\rangle\rangle$, i.e. the probability density of observing staircase microbarriers as a function of ambient gradient drive. This *'ambient drive'* $\langle\langle \nabla T/T\rangle\rangle \equiv \nabla\langle\langle T\rangle\rangle/\langle\langle T\rangle\rangle$ is the temperature gradient length at the location of the corrugation, should this corrugation not exist [20]. Practically, it is computed from the time-averaged and radially-smooth temperature profile $\langle\langle T\rangle\rangle$—hereafter referred to as *'background'*, or *'ambient'* state—with corrugations removed, i.e. smoothly interpolated at the location of corrugations from the temperature profile on both sides of the corrugation[3].

The data in figure 4 is based on the flux-driven data of figure 2 during 6500 c_s/a, with $c_s = (T_{e,0}/m_i)^{1/2}$ the sound speed evaluated at mid-radius, T_e the electron temperature and m_i the ion mass. In this dataset, $\langle\langle R/L_T\rangle\rangle$ varies with time and radius between $\langle\langle R/L_T\rangle\rangle = 3$ close to the source region $\rho \sim 0.3$ and $\langle\langle R/L_T\rangle\rangle = 9$ near to the edge $\rho \sim 0.85$. Regardless of the precise choice for the selected computation, main features in figure 4 are robust.

Clearly, staircase organisation exists in a precise range of gradient drives, here: $\langle\langle R/L_T\rangle\rangle \in [5, 8]$. Let us call 'marginality'

[3] Anticipating results below, in gradient-driven computations (see appendix A for definitions) as no corrugations may develop, by definition $\langle\langle R/L_T\rangle\rangle$ coincides with the time-averaged R/L_T. In the flux-driven case $\langle\langle R/L_T\rangle\rangle$ is very close to the time-averaged gradient-driven R/L_T everywhere except in the vicinity of profile corrugations (staircase steps), as shown in figure 15(a), bottom panel.

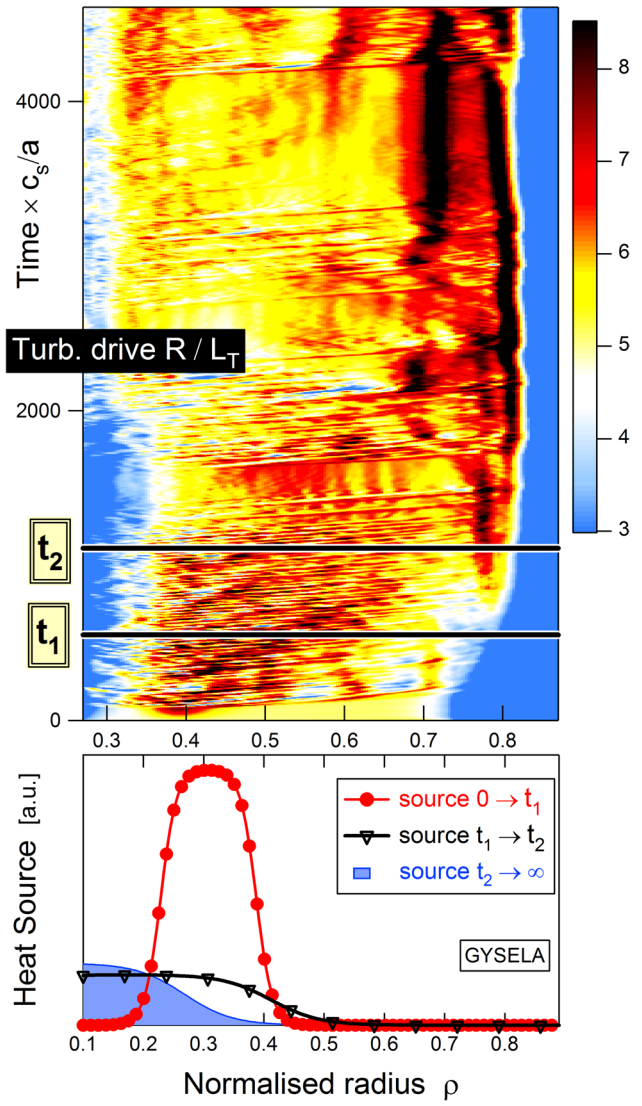

Figure 5. A numerical experiment to illustrate the importance of proximity to marginality for staircase onset and development and the importance of avalanching for relaxation.

(or 'criticality') the normalised gradient at which the turbulent heat flux becomes greater than the neoclassical heat flux. The turbulence-dominated regime starts at marginality. $\mathbf{E}\times\mathbf{B}$ staircase onset is a near-marginal phenomenon, residing in the low-heating limit [20, 30] of flux-driven forcing. Some turbulence activity is indeed necessary to fuel the positive feedback between zonal mean flows and mean profile corrugation (sections 1.2.1 and 2.2) and allow for the staircase onset. Starting at flux-driven marginality $\langle\langle R/L_T^{\text{F-D}}\rangle\rangle \approx 3.8$ and increasing the gradient drive, a narrow region $\langle\langle R/L_T\rangle\rangle \in [3.8, 5]$ of intermittent turbulence activity is thus first found before entering the 'staircase regime' $\langle\langle R/L_T\rangle\rangle \in [5, 8]$. In that region $\langle\langle R/L_T\rangle\rangle \in [3.8, 5]$ avalanches carry a non-vanishing turbulent heat flux, even at vanishing collisionality [31]. The system is strongly intermittent, mean flows are rapidly destroyed and turbulence is regulated by fluctuating zonal disturbance flows (see appendix A for definitions). When entering the staircase regime, the flux-gradient relation is modified and heat transport is now controlled by the staircase shear layers, as illustrated in figure 15. Farther from marginality (here above $\langle\langle R/L_T\rangle\rangle \gtrsim 8$), free energy is large, staircase organisation is progressively destroyed and flux- and gradient-driven transport are expected to become more similar. Staircase organisation thus appears as a natural tendency for the near-marginal turbulent system.

To further illustrate this near-marginal character, the following numerical experiment is run, summarised in figure 5. Collisionality is moderate: $\nu_\star = 0.1$ (see next section 1.2) and kept constant across the radius so that collisional damping of zonal flows is weak and comparable between core and edge. The safety factor is parabolic and monotonically increasing between $q = 1.16$ at the centre and 2.4 at $\rho = 0.9$. A strong transient initial heat source centred around $\rho = 0.3$ (bottom figure) is incrementally decreased in amplitude and shifted radially at times $t_1 = 553\, a/c_s$ and $t_2 = 1111\, a/c_s$. The idea is to investigate in a test case with homogeneous zonal flow damping the dynamics of turbulence organisation as the temperature profile reorganises.

In the initial stage $t \in [0, t_1]$, driven by the strong source, the temperature gradient transiently increases far above marginality $\langle\langle R/L_T\rangle\rangle \sim 9 - 10$ in the central region $\rho = 0.3 - 0.5$ resulting in a strong avalanching activity clearly visible in figure 5 until a little after t_2. Even though at time t_1 the source is reduced, the system unsurprisingly responds with a time delay to the strong initial drive. Unsurprisingly also, the dominant mechanism through which the plasma disposes of its large free energy content is through the *emission of heat avalanches*, i.e. through intermittent *mean profile relaxations*. Through avalanching the system becomes *stiff*: this mechanism is faster and more efficient than relying upon diffusion to mitigate developing strong gradients.

Whilst the supercritical core region intermittently responds to the strong energy injection, the edge region between $\rho = 0.7 - 0.8$ is close to criticality with gradient drives $\langle\langle R/L_T\rangle\rangle$ in the range between 3 to 6 [the linear instability threshold is around 4.5]. Given these conditions the first staircase step is observed to nucleate around time $t = 830\, a/c_s$ and close to $\rho = 0.8$, a location uncorrelated to a low-order q rational (section 3.1). As the source decreases the temperature gradient reorganises, relaxing outside-in towards criticality. Following the relaxing temperature gradient (section 3.2), the staircase also builds up outside-in as larger regions of the plasma become near-critical.

The intermittent character of the system (generic even though especially visible in the early stages of this experiment and close to the source region) is not deeply modified by the emergence of the staircase pattern. Intermittency remains through avalanche emission a key manifestation of the system, see e.g. [7, 32–34]. The onset of the staircase pattern however does mitigate the radial extent of the propagating heat avalanches [1], allowing for better heat confinement as the pattern builds up. This point is specifically discussed in sections 2.3 and 2.4 and differently illustrates the somewhat counter-intuitive idea present in figure 15 that a system (flux-driven) described by strongly non-Gaussian statistics may have better confinement properties than a related system (gradient-driven) that is statistically closer to Gaussianity.

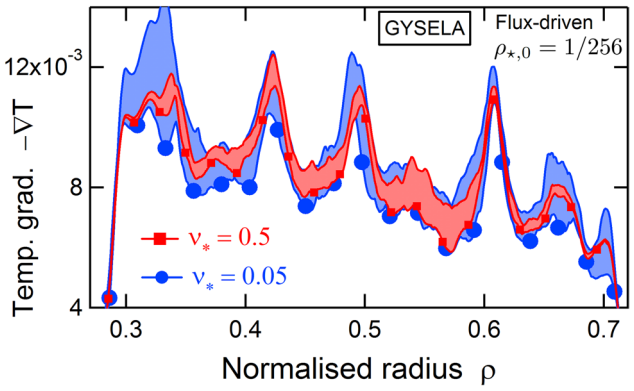

Figure 6. Staircase organisation is weakly affected by collisionality $\nu_\star$ in the banana regime (weak zonal flow damping). Collisionality here is constant across radius.

The essential difference residing in the microbarrier patterning, constitutive of the staircase.

1.2. A low-collisionality pattern

Zonal flows are linearly damped through collisions alone [24]. Steps of an $\mathbf{E}\times\mathbf{B}$ staircase constitute an organised pattern of zonal mean flows (see also section 2.2). An upper bound on collisionality (on the strength of collisional dissipation) is expected for this pattern to exist. Scans in collisionality, in varying plasma conditions are now discussed.

1.2.1. Commonly observed at low collisionality. In the low-collisional banana regime [35] (normalised ion–ion collisionality $\nu_\star \leqslant 1$), extensive scans in collisionality in the range $\nu_\star \in [0.001, 0.5]$ have consistently shown a weak or negligible impact of this parameter on staircase organisation. An example is shown in figure 6 where two computations are compared, differing through a tenfold increase in collisionality. In realistic cases collisionality significantly varies across the radius, following density n, temperature T, safety factor q and aspect ratio $\epsilon^{-1} = R/r$ variations as typically shown in figure 9 (inset):

$$\nu_\star = \frac{qR_0}{v_T}\frac{\nu_{ii}}{\epsilon^{3/2}}, \quad \text{with } \nu_{ii} = \frac{4\sqrt{\pi}}{3}\frac{n\,e^4\log\Lambda}{(4\pi\epsilon_0)^2\,m^2\,v_T^3} \qquad (1)$$

the ion–ion collision frequency, $v_T = (T/m)^{1/2}$ the thermal velocity, R the major radius, ϵ_0 the permittivity of free space and $\log\Lambda \approx 17$ the Coulomb logarithm [36, 37]. In the computations of figure 6, in contrast with the rest of the paper, collisionality is artificially set constant across the radius to precisely test the impact of collisional dissipation on the flow and profile organisation, disentangled from its profile variations.

Fluctuations of the temperature gradient are shown during respectively one collision time ($\nu_\star = 0.5$) and 0.6 collision time ($\nu_\star = 0.05$). As expected, the magnitude of shear at the staircase steps is slightly larger at weaker collisionality; corrugations are also slightly more marked. The overall influence however of $\nu_\star$ on staircase organisation is weak in the low-collisional banana regime.

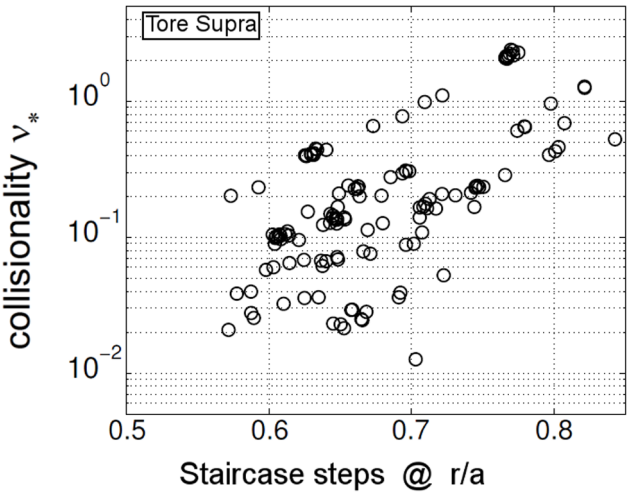

Figure 7. Experimental observation of staircase corrugations as a function of collisionality and radial location in Tore Supra. Staircases have only been observed so far in the low-collisional banana regime, supporting calculation predictions (see figure 8).

Experimentally, core plasma main ions are typically in banana regime. Staircase signatures are common there, as shown from the Tore Supra data in figure 7, processed for staircase identification as detailed in [20, 21]. About 200 experimental staircase signatures are shown. Interestingly, such signatures disappear at the banana-plateau transition (around $\nu_\star \approx 1$) and none has been observed so far in the plateau regime, $\nu_\star \gtrsim 3$–4, an indication confirmed by computations (see following section) that collisionality starts playing an important role at the banana-plateau transition (hence will play a role closer to the plasma edge region) through effective damping of the staircase microbarriers.

1.2.2. Disappearance at higher (plateau) collisionality. Ubiquitous in the low-collisional banana regime, staircase organisation progressively disappears in the range $\nu_\star \in [1, 5]$ at the banana-plateau transition. Identification of staircase-like structures in plateau collisional regimes is hardly possible due to the increased collisional dissipation and hence short zonal mean flow lifetime. Figure 8 shows the behaviour of a step layer whilst crossing the banana-plateau transition. The low-collisional banana regime computation (left panel, $\nu_\star = 0.15$ at $\rho = 0.3$) exhibits the typical staircase pattern discussed above. We show here the detail of one of its shear layers around $\rho = 0.25$, with complex merger and division dynamics. The right panel shows an otherwise identical computation, except for a tenfold increase in collisionality (plateau regime, $\nu_\star = 1.5$ at $\rho = 0.3$). The time interval for which data is displayed and the colourbars are identical. As expected, both mean and disturbance $\mathbf{E}\times\mathbf{B}$ shear are weaker in the plateau regime. Interestingly, fluctuations in temperature remain mostly unchanged in magnitude by the tenfold increase in collisionality but as the shear pattern is collisionnally damped mean corrugations are weaker, emphasising the *positive feedback that mean shear provides on profile corrugation*.

The progressive weakening of staircase organisation as collisionality increases also translates into better confinement at

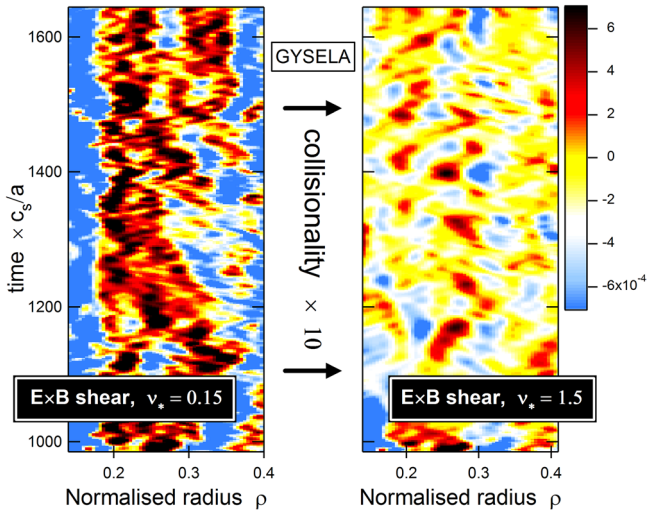

Figure 8. Impact of collisional dissipation on the $\mathbf{E} \times \mathbf{B}$ staircase. The pattern exists in the low-collisional banana ($\nu_\star = 0.15$) limit of magnetised plasma turbulence and starts disappearing at the plateau transition ($\nu_\star = 1.5$).

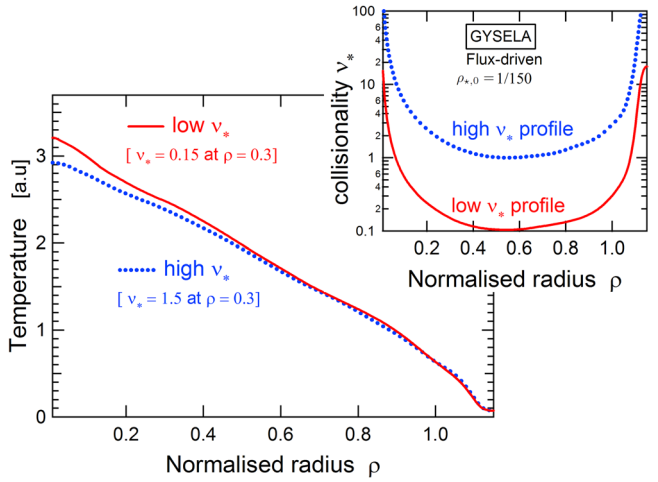

Figure 9. Temperature and collisionality profiles of figure 8 in banana and plateau regimes for the otherwise same plasma parameters. Confinement degrades and the central temperature drops by about 10% as the staircase pattern starts disappearing at higher collisionality.

low collisionality, as shown in figure 9 for the same dataset. Less collisional plasmas lead to stronger $\mathbf{E} \times \mathbf{B}$ staircase patterning. In the setup of figures 8 and 9 a tenfold decrease in collisionality leads to at least a 10% increase in central temperature (flux-equilibrium is not yet reached for the low $\nu_\star$ case: the temperature profile is still slowly building). The observed discrepancy in profiles between the two computations (banana versus plateau) overlaps with the region of staircase activity, i.e. from $\rho = 0$ to around $\rho = 0.6$, the outermost radial location of the low-collisional $\mathbf{E} \times \mathbf{B}$ staircase step. Staircase onset with its successive microtransport barriers is thus directly responsible for confinement improvement at low collisionality.

1.3. Partial summary and outlook

The beneficial (see following sections) $\mathbf{E} \times \mathbf{B}$ staircase patterning is primarily a core phenomenon because of the conjunction of both low collisional dissipation and proximity to marginal stability. However depending on the plasma parameters, $\mathbf{E} \times \mathbf{B}$ staircase organisation may appear and develop anywhere within the plasma if the conditions are right, as e.g. illustrated in figure 5. Also, as a *near-marginal and low-collisional* feature of magnetised plasma turbulence staircase organisation may be especially relevant for the confinement of current and next-generation large (near-marginal) and hot (collisionless) fusion devices.

2. Staircase organisation matters

Previous sections have emphasised why global staircase organisation may be relevant to large machines and hot core plasma conditions. We now detail how such organisation, result of a balanced interplay between extended avalanches and localised microbarriers, impacts quantities relevant for confinement:

- the organised pattern of microbarriers impacts heat transport;
- the positive feedback between mean $\mathbf{E} \times \mathbf{B}$ flow and mean profiles modifies the spatial distribution of shear and its temporal coherence in computations;
- strength and steadiness of the staircase organisation (of its microbarriers) provides a favourable gyro-Bohm-like scaling for confinement; unsteadiness and weakening of this organisation (of the microbarriers) a route to gyro-Bohm breaking.

To illustrate these points we compare with the same tool two modeling frameworks. 'Flux-driven' is first run as reference and is the usual running mode of GYSELA. Then 'gradient-driven' computations are compared to this reference case; they only differ from the flux-driven framework through a constrained exploration of phase-space, the background (or 'ambient' in the sense defined on page 3) plasma parameters are the same. In particular the flux-driven approach sets no constraints upon large-scale avalanche-type front propagation and allows for consistent feedback between flows, shear and mean profiles. Staircase organisation clearly depends on the latter, possibly on both. Details and further discussion can be found in appendices A and B.

2.1. Staircase hindered in gradient-driven forcing

Space and time characteristics of the self-organised turbulent state is compared in figures 10 and 11 for flux- and gradient-driven regimes with identical plasma parameters, in the banana collisional regime ($\nu_\star = 0.2$ at $\rho = 0.5$). The flux-driven computation is first run up to flux equilibrium. Based

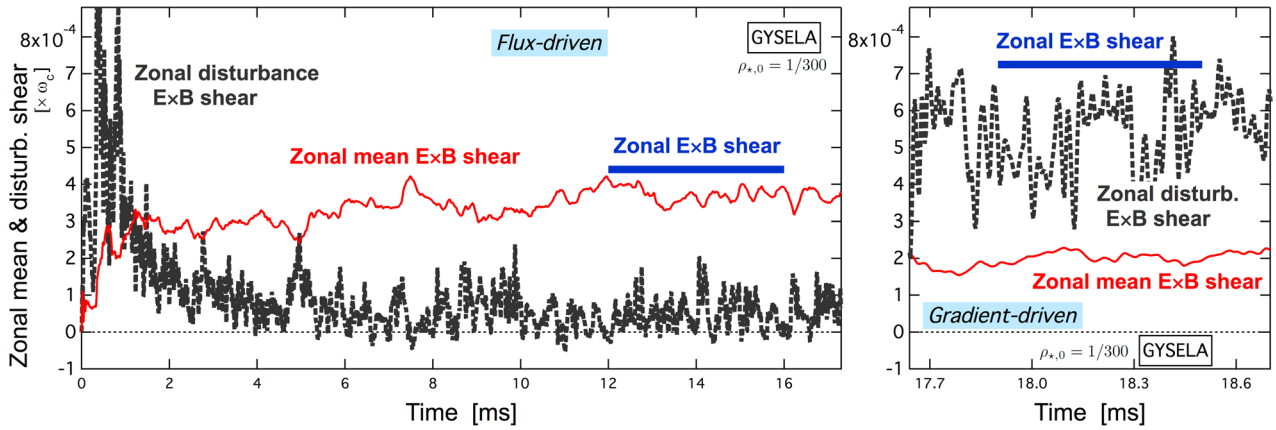

Figure 10. Comparing zonal disturbance (black) and zonal mean shear (red) averaged radially from $\rho = 0.4$ to 0.8 in flux- and gradient-driven frameworks. Mean is defined through sliding time averages of 0.3 ms. For each case the steady-state zonal shear magnitude (disturbance plus mean, thick blue) is indicated (time averaged between 12 and 16 ms (left); between 17.9 and 18.5 ms (right)). Corresponding levels of turbulence $(\delta\Phi^2)^{1/2}$ are shown in figure 26. The average gradient-driven zonal shear magnitude (resp. turbulence intensity) is 40% (resp. 15–20%) larger than its corresponding flux-driven counterpart.

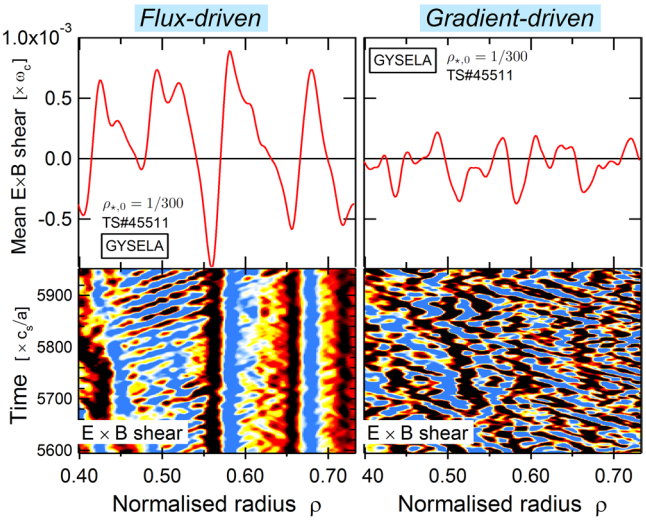

Figure 11. The mean $\mathbf{E} \times \mathbf{B}$ shear, averaged over 0.3 ms (1 collision time at $\rho = 0.5$) is shown in both flux- and gradient-driven computations that display comparable turbulence intensities (see figure 26). No perennial structures genuinely endure in the gradient-driven approach, mean components are vanishing and the staircase pattern is lost.

on the end state at 17.4 ms, the computation is then restarted in gradient-driven mode, details of the procedure are given in appendix A.

The staircase pattern visible in figure 11 that has built up and endures in the flux-driven computation is rapidly (in less than a millisecond) damped away and ultimately lost in the gradient-driven approach. The time interval and colourbars for which data is displayed in figure 11 are identical. The temperature corrugations and strong inhomogeneities in mean shear and poloidal flow, characteristic of the staircase pattern give way in the gradient-driven framework to a more homogeneous turbulence, with fluctuations more isotropic, flow and shear patterns more random in time and evenly distributed poloidally.

The fact that front propagation is also visible in the gradient-driven framework emphasises its generic character as a means of transport. Yet major differences exist with the flux-driven avalanching behaviour: (i) fronts occur because mean profiles depart from equilibrium; the back-reaction however on the mean profiles that allows for nonlinear transport feedback is discarded in the gradient-driven context due to the restoring force with strength γ^K in equation (A.2). This restoring force contributes to (ii) damping the fronts as they propagate through de-synchronisation of the profile fluctuations (the restoring force acts with a short time delay against the fluctuating dynamics). This randomness of the restoring force in both space and time (iii) implies a similar randomness for the fronts, in time as well as in size and in direction and extent of propagation. Section 2.4 further highlights a possible consequence of avalanches for transport.

2.2. Staircase: a signature of modified zonal flow characteristics

An important point for transport prediction is related to $\mathbf{E} \times \mathbf{B}$ shear. The total amount of shear that is actually generated is of course an important quantity but as well its spatial distribution and temporal coherence: the more concentrated and the longer-lived, potentially the more effective. We now show, comparing flux- and gradient-driven frameworks how the interplay of turbulence fluctuations and mean profiles has non-trivial consequences on the space–time distribution of zonal flow shear. This has an impact on heat transport which the following section 2.3 details.

Zonal flows (ZF) are the axisymmetric component of $\mathbf{E} \times \mathbf{B}$ flows [10]. They can be decomposed into mean and disturbance. 'Mean' is defined as the low frequency, slow-evolving component of the zonal flows through sliding time averages of 0.3 ms or longer (0.3 ms corresponds to 1 collision time at $\rho = 0.5$). An unambiguous designation is as 'zonal mean flows' and 'zonal mean flow shear', often abbreviated to 'mean flow' (MF) and 'mean shear'. The disturbance part ('zonal disturbance flows' and 'zonal disturbance shear') is simply defined as the remaining part of the zonal flows with

dynamic evolution on shorter time scales than 0.3 ms. It is abbreviated to 'disturbance flows' and 'disturbance shear'. Importantly, this definition holds *without restriction to small-amplitude disturbances*. With a longer time averaging of 0.6 ms, the coherence of mean shear is further reduced in the gradient-driven calculation whilst it remains essentially unchanged in the flux-driven case—figure 15 for instance, bottom panel, still shows staircase organisation after ∼3 ms of temporal averaging despite its meandering behaviour illustrated in section 3.2.

2.2.1. Prominence of zonal mean flows. Figure 11 displays the radial profile of mean shear in both flux- and gradient-driven frameworks whilst figure 10 shows the time evolution of radially-averaged absolute mean shear $\langle|\langle\gamma_{\mathbf{E}\times\mathbf{B}}\rangle_\tau|\rangle_r$ (solid red) and disturbance (dotted black), with $\langle\cdot\rangle_\tau$ denoting the 0.3 ms sliding time average and $\langle\cdot\rangle_r$ the radial averaging from $\rho = 0.4$ to 0.8. The zonal shear magnitude (solid blue, sum of mean and disturbance) is indicated in steady-state, respectively averaged between 12 and 16 ms and between 17.9 and 18.5 ms. From both figures, several features stand out:

Gradient-driven: The fluctuating, randomly varying disturbance shear is the dominant contribution to zonal shear in the gradient-driven approach. The disturbance shear is homogeneously distributed spatially. As expected from the restoring force in equation (A.2), beyond a few collision times the gradient-driven mean shear is damped and spatially homogenised. Gradient-driven zonal shear is thus spatially homogeneous (all radial locations are equivalent) beyond a few collision times;

Flux-driven: In contrast, the dominant contribution to zonal shear in the flux-driven approach is as coherent mean shear. For the staircase pattern to form and mean shear to endure, positive feedback between flow and gradient is required. Being uncorrelated at its inception to low-order q rationals (section 3.1) mean flow localisation is spatially equiprobable. Mean profile corrugation provides the seed for mean flow localisation through spatial symmetry breaking. The mean flow then locks-in the corrugation through reduction of transport. Positive feedback between the zonal mean flow and the mean plasma gradient allows for strong spatial localisation of staircase microbarriers. There, locally, zonal shear is 2 to 8 times larger than in the gradient-driven case. In a staircasing flux-driven regime the dominant contribution to zonal shear thus comes from narrow regions of concentrated zonal mean shear. In-between staircase steps zonal shear is small, randomly fluctuating and dominantly carried by the disturbance part;

Confinement efficiency: The total magnitude of zonal shear (mean plus disturbance) generated in the gradient-driven framework is ∼40% larger than in the reference flux-driven case. This may result from the 15–20% larger gradient-driven turbulence intensity, see figure A3 (hence stronger zonal flow drive). However, as next section 2.3 highlights, stronger zonal flow magnitude *does not* translate into better confinement in the gradient-driven case. The opposite is observed, suggesting that the rapidly varying zonal disturbance flows are less effective than zonal mean flows in regulating transport. An efficient confinement is thus best achieved for a given level of zonal flow activity through a staircase (mean flow dominated) type of organisation.

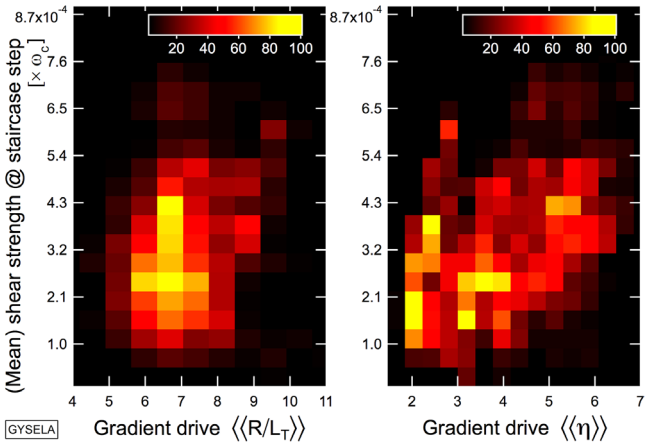

Figure 12. Strength σ_{step} of staircase shear layers as a function of gradient drive (distance to marginality).

2.2.2. Microbarrier strength and permability. Further important points regarding zonal shear organisation are how microbarriers are modified with varying gradient drive (with distance to marginality) and with varying machine size $\rho_\star$. To this end, as is done in figure 4, we track in time the location of the staircase steps r_{step} and compute there the zonal mean shear strength σ_{step}:

$$\sigma_{\text{step}}(r_{\text{step}}, t) = \int_{r_{\text{step}}-\delta^{\text{flow}}/2}^{r_{\text{step}}+\delta^{\text{flow}}/2} \frac{\mathrm{d}r'}{\delta^{\text{flow}}} \left|\langle\gamma_{\mathbf{E}\times\mathbf{B}}\rangle_\tau(r', t)\right| \qquad (2)$$

with $\delta^{\text{flow}} \sim 10\,\rho_s$, as shown in [20, 21]. The integration interval in equation (2) corresponds to the radial width of the staircase microbarriers so physically σ_{step} is a proxy for microbarrier strength, i.e. for how impermeable microbarriers are to radial transport or how effective they are as barriers for transport.

Since $r_{\text{step}}(L_T, L_n)$ is a function of the temperature and density gradients σ_{step} can be displayed as a function of the ambient (see definition above, section 1.1) gradient drive $\langle\langle R/L_T\rangle\rangle$, or to incorporate the effect of a varying density gradient as a function of $\langle\langle\eta\rangle\rangle = \langle\langle L_n/L_T\rangle\rangle$. This is shown in figure 12. Binning is applied, the colourscale represents how often a given binned σ_{step} value is found (the most encountered value is normalised to 100). Interestingly, zonal mean shear strength increases with increasing gradient drive, but stability of the microbarriers decreases with increasing gradient drive. In other words, increasing gradient drive generates increasingly strong microbarriers but with decreasing probability to endure, again emphasising the near-marginal character of staircase organisation.

Similarly, figure 13 displays σ_{step} as a function of $\rho_\star^{-1}$ and predicts an unfavourable scaling of staircase microbarrier

strength with increasing $\rho_\star^{-1}$. This result suggests an increased permeability of the staircase microbarriers with $\rho_\star^{-1}$, i.e. a decreasing barrier strength with increasing plasma size. Interestingly, this result echoes recent experimental findings—figure 3 in [21]—and may provide pathways to understand the observed weakening of gyro-Bohm scaling [38] at relevant large $\rho_\star^{-1}$, although this weakening may be balanced by the mechanical increase of the number of staircase steps with increasing $\rho_\star^{-1}$. A critical question for transport scaling with $\rho_\star^{-1}$ is that of the trade-off between unfavourable microbarrier weakening and beneficial increase in the number of staircase steps. This topic is further discussed in section 2.4.

2.3. Impact on profile stiffness and heat fluxes

Let us call *local flux-gradient relation* the often postulated instantaneous bijection that may exist between the local values of fluxes (of particle, heat, momentum) and the local values of the gradients (∇T_i, ∇T_e, ∇n). In this framework, above a critical threshold:

(ɦ1) a given normalised gradient will drive a unique time-averaged level of flux,

(ɦ2) a non-vanishing level of flux is in unique correspondence with a single linear combination of normalised gradients—the flux-gradient relation is then called 'single-valued' and

(ɦ3) there is no time delay between modification of a normalised gradient and response of the corresponding flux(es).

Known issues may lead to the breakdown of this representation: (i) additional control parameters may enter the flux-gradient relation—e.g. zonal flow strength, sketched in figure 14 may introduce a nonlinear dependence on the gradients, induce a transport bifurcation [39, 40] or play a different role for transport depending on distance to marginal stability as illustrated through the observation of staircase organisation, (ii) nonlocal features appear—e.g. the local value of a flux depends on the state of the system in distant regions of space, or on its past history or (iii) a time delay appears in the response of a flux to a modification of the gradients—a weak form of temporal nonlocality.

The local flux-gradient relation is based on Fourier's or Fick's laws for transport and is a common rationale for drift-wave turbulence, usually verified in gradient-driven modeling as e.g. explicit in [26]. From it stems the notion of *stiffness* which quantifies the (local) rate of change of a (local) flux with respect to the difference between its (local) driving normalised gradient and the (local) instability threshold [41].

Even within validity of the local flux-gradient relation, structure formation and especially the onset of zonal flows is known to significantly impact stiffness [42]. Staircase patterning is a signature of modified shear-gradient interplay. It is thus certainly natural to expect in its presence a modified flux-gradient relation as well. A precise discussion of these matters is left for future work. We focus here on an intermediate problem and show that despite similar ambient gradient drives, predicted heat fluxes are significantly different in a gradient-driven framework with no staircase organisation and in a flux-driven framework with staircase organisation.

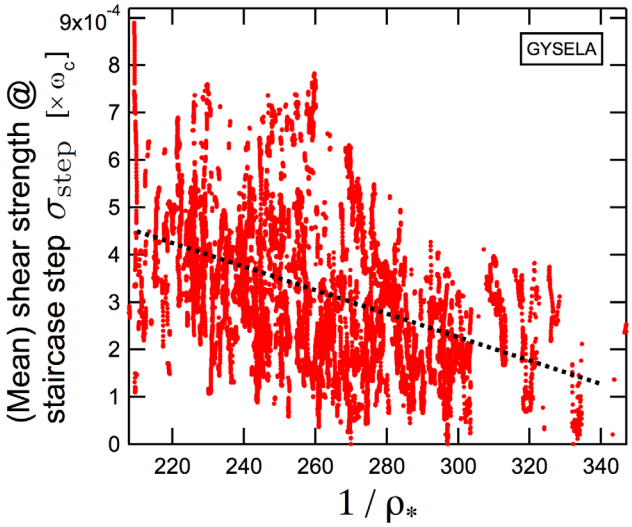

Figure 13. Strength (impermeability) σ_{step} of staircase shear layers as a function of machine size $\rho_\star^{-1}$. The least-squares regression is shown in dotted black.

In a flux-driven framework, the power $\mathcal{P} \propto rQ$ flowing through successive flux surfaces is approximately constant at flux equilibrium, Q being the total heat flux, sum of a turbulent flux (associated to the $\mathbf{E} \times \mathbf{B}$ drift) and of a curvature flux (associated to the curvature and grad-B drifts). Though their sum is monotonically constrained at equilibrium, flux-driven turbulent and curvature fluxes may vary somewhat independently. In a flux-driven context the *total* equilibrium heat flux is constrained by the (constant or slowly-varying) source. It is an essential difference with gradient-driven frameworks in which fluxes are not *a priori* bounded and respond to the time-radius adaptive force equation (A.2) that maintains ambient mean profiles—see figure A2 and appendix A for details. It is thus of special relevance to investigate flux responses in these two frameworks, especially close to marginal stability where transport is often reported to be *stiff*, i.e. where small variations in gradient drive may be responsible for large excursions of fluxes.

To this end we compare in figure 15 predictions for the turbulent heat fluxes at the same successive radial locations in both flux- and gradient-driven frameworks. The ambient gradient drives are comparable in both cases and near-marginal. Staircase organisation is absent in gradient-drive and visible in the flux-driven case through its shear layers (steps 1 to 3) marked as R/L_T corrugations. The corresponding gradient-driven R/L_T profile with no staircase is non corrugated. Turbulence characteristics are quasi-steady—figure 15 displays results averaged over 2.95 ms (1033 c_s/a).

- Location [0] is a region of low linear drive, prior to entering the staircase region located between $\rho = 0.4$ and 0.8. The average flux-driven (black square) and gradient-driven (blue circle) heat fluxes are small and comparable, yet with a marked intermittent character and a large statistical variability for the flux-driven turbulent heat

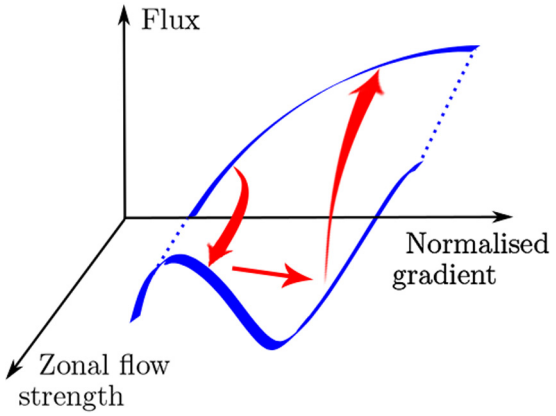

Figure 14. Example of breakdown of local flux-gradient relation: as the system evolves (red arrows) the flux-gradient landscape is modified by a third control parameter (here zonal flow strength) from single-valued to multi-valued and back to single-valued at large normalised gradient drive.

flux, even at weak gradient drive $R/L_T \approx 5$. This is unlike common representation of near-marginal ITG transport [26] and will be discussed elsewhere;

- Locations [1], [2] and [3] are respectively after 1, 2 and 3 successive staircase steps. As more of the staircase barriers are crossed computed heat fluxes start to significantly differ despite comparable ambient gradient drives. Both radial heat flux profiles are radially smooth, as expected. Where the gradient-driven flux monotonically increases with increasing gradient drive R/L_T, the flux-driven flux does not and radially organises so as to satisfy the flux-equilibrium condition $\mathcal{P} \approx$ constant.

Several conclusions can be drawn:

(i) *the gradient-driven framework appears to be overly stiff*: predicted flux levels are too large in gradient-driven modeling, especially near marginal stability;

(ii) strong stiffness endangers predictive reliability in a model as large variations in predicted fluxes can be obtained from modest or even possibly indistinguishable differences in ambient mean profiles (within statistical fluctuations or experimental error bars). *Reliability of gradient-driven predictions near marginal stability is thus questioned*. The flux-driven framework is less stiff and appears less sensitive to details of the ambient mean profiles;

(iii) these observations may have implications for the so-called 'transport shortfall' problem [43, 44]. Strong stiffness indeed impedes nonlocal turbulence propagation and especially turbulence spreading [45], a possibly important ingredient to the shortfall problem [46];

(iv) the fact that large though highly intermittent flux-driven fluxes are observed at low temperature gradient drives (location [0]) where both the gradient-driven flux and its statistical variations remain small tends to indicate clear sensitivity of the flux-gradient relation to temporal coarse-graining, despite the fact that the present results are flux-surface averaged and thus already strongly spatially coarse-grained. This result echoes results in [47, 48]. *The local flux-gradient relation is violated (becomes multivalued) in a flux-driven framework at short to intermediate (collisional) time scales*, hence questioning hypothesis (ħ2) above;

(v) our understanding of near-marginal stiffness is clearly questioned and echoes the recent observation of an increased nonlinear upshift of the temperature gradient length threshold, attributed to $\mathbf{E} \times \mathbf{B}$ staircase onset [30]. These questions point towards the role of staircase organisation and generally of structure formation near marginal stability in the possible breakdown of the local flux-gradient paradigm, as sketched in figure 14. As such they may be seen as a generalisation of earlier heuristic models where e.g. the heat diffusivity $\chi = -Q/\nabla T$ is itself a nonlinear function of either zonal flow shear [13] or of ∇T itself.

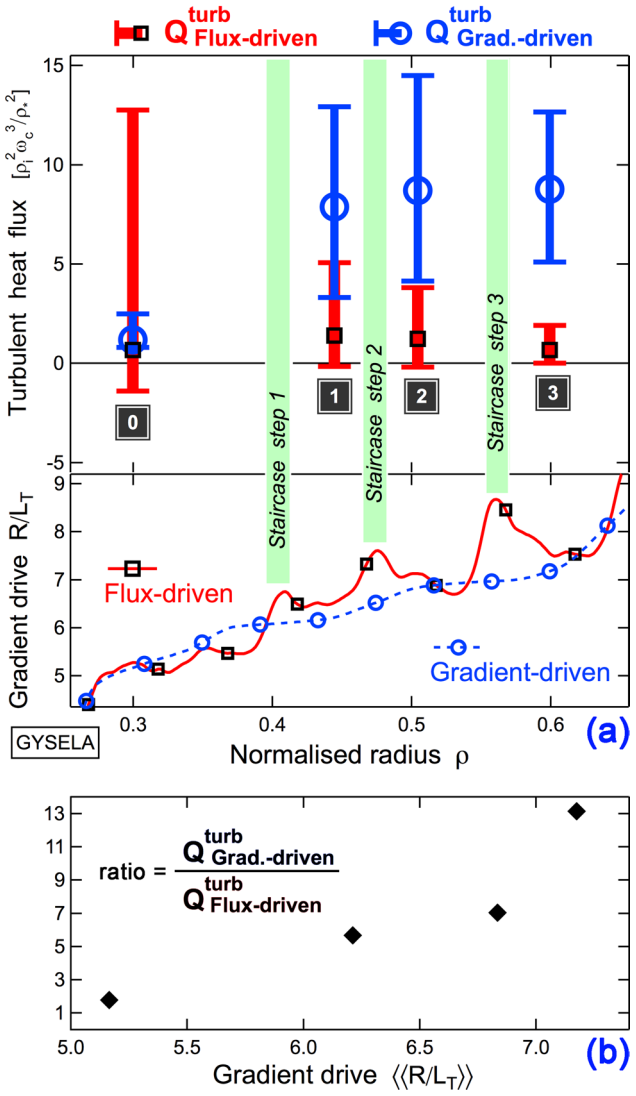

Figure 15. Turbulent heat fluxes before [0] and after [1], [2] and [3] staircase steps in the flux-driven approach, compared to turbulent heat fluxes at the same locations in the gradient-driven case, figure (*a*). Same data, shown as the ratio of gradient-driven to flux-driven predictions for the heat flux as a function of ambient gradient drive, figure (*b*). The increasing discrepancy with $\langle\langle R/L_T \rangle\rangle$ between both predictions illustrates issues with gradient-driven predictions of near-marginal transport and stiffness.

In the above respects, *a local flux-gradient relation is a poor description of flux-driven near-marginal transport*. Trying to describe through this simplified framework the variety of near-marginal transport processes is likely to *increase complexity* in the long run and be responsible for transport processes to become overly sensitive to details of the mean gradients. Stiffness may be an example of this increased complexity since with no clear physical motivations, it is reported to strongly vary with plasma parameters [49] or regions of the plasma [50].

A paradigm change, or at least additional dimensions in the usual flux-gradient framework (as e.g. in figure 14) certainly appears desirable to restore simplicity in describing transport and encompassing the reality of structure formation (zonal flow, staircase, etc) near marginal stability. This question is left for future work.

2.4. Possible routes to confinement improvement... or to gyro-Bohm breaking

Previous sections have established staircase step layers as efficient microbarriers for transport. We now characterise transport in-between these microbarriers and investigate its possible consequences for global confinement.

2.4.1. The staircase steps contain the avalanche activity. In-between staircase steps the transport of heat or momentum dominantly occurs through avalanche-type processes. Avalanches lead to strongly non-Gaussian statistics with a marked Lévy-type non-local, non-diffusive character [1]. In the *absence of regulating mechanisms for avalanches* a departure from favourable gyro-Bohm confinement scaling is thus expected. *The* $\mathbf{E}\times\mathbf{B}$ *staircase organisation is especially relevant because its microbarriers are efficient avalanche regulators*. This was noted in [1], figure 2 and is further shown in figure 16.

To illustrate this point, we isolate a $100\,a/c_s$ time window during which the staircase organisation is steady. There we compute the Lagrangian space-time autocorrelation $\mathcal{A}$ of the turbulent heat flux in two distinct regions of the plasma chosen such that (i) both regions are bounded by steady staircase microbarriers and (ii) the radial width Δ between these microbarriers is significantly different in both cases. Each of the two regions is a different 'tread' of the staircase as defined in figure 1; their width Δ is practically measured as the distance between the bounding temperature corrugations. The first region shown in figure 16(a) has a width of $\Delta = 58\,\rho_s$, the second region in figure 16(b) a large width of $\Delta = 153\,\rho_s$.

Individually, avalanches are hard to systematically track. Statistically, the radial extent of space-time autocorrelation measures the coherence of radial heat transport. The full width at half maximum of $\mathcal{A}$ (black contours) is thus an estimate for the avalanche size in both cases (a) and (b). Interestingly, the full width at half maximum of $\mathcal{A}$ closely tracks, *in both significantly different cases* (a) and (b) the local step size of the staircase. This leads to the following conclusions:

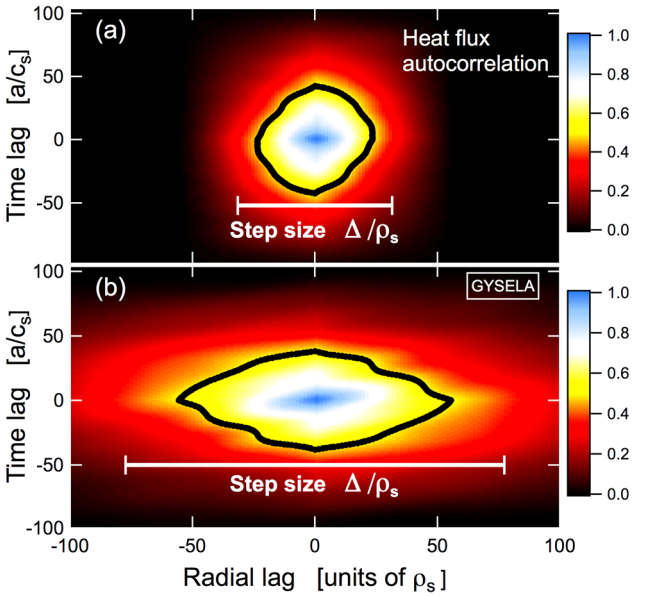

Figure 16. Autocorrelation of the turbulent heat flux in two separate radial regions of the plasma, at the same time, during $100\,a/c_s$: case (a) in-between two staircase steps distant of $\Delta = 58\,\rho_s$ and case (b) distant of $\Delta = 153\,\rho_s$ (shown as white interval). In both cases the full width at half maximum (black contour), a measure of the radial coherence of heat transport, tracks well the local staircase step width.

- the staircase step size Δ (easy to measure) is a good proxy for the radial extent of avalanches;
- avalanche activity is a route to *gyro-Bohm breaking*: in two distinct regions of the plasma and at the same time, the turbulent heat flux has at least *three different radial scalings*: two mesoscale ones associated to staircase organisation $\sim 50\rho_s$ and $\sim 150\rho_s$, in addition to the robust local $\ell_c \sim 6\rho_s$ scale (see figure 3);
- regardless of the step size (the 'tread width'), avalanche transport fills-in the 'treads'. Without staircase microbarriers avalanches would thus propagate unhindered across larger portions of the unstable plasma domain. As a consequence, *stable staircase microbarriers are efficient regulators for the radial propagation of avalanches.*

2.4.2. Statistics of staircase step sizes. The relative strength of beneficial microbarriers and detrimental avalanches evolves dynamically, as both interplay: avalanches are dominantly emitted on both sides of temperature corrugations whilst larger avalanches cause microbarriers to meander (see section 3.2) or be destroyed. Determining which of the two dominates in what region of parameter space may open new routes to access and possibly control:

- improved confinement: favoured in the case of strong, steady and closely packed microbarriers. An interesting perspective being that these microbarriers may coalesce [14, 21] into larger scale macrobarrier(s). Whether observations in [51] are a manifestation of such phenomena is yet unclear;

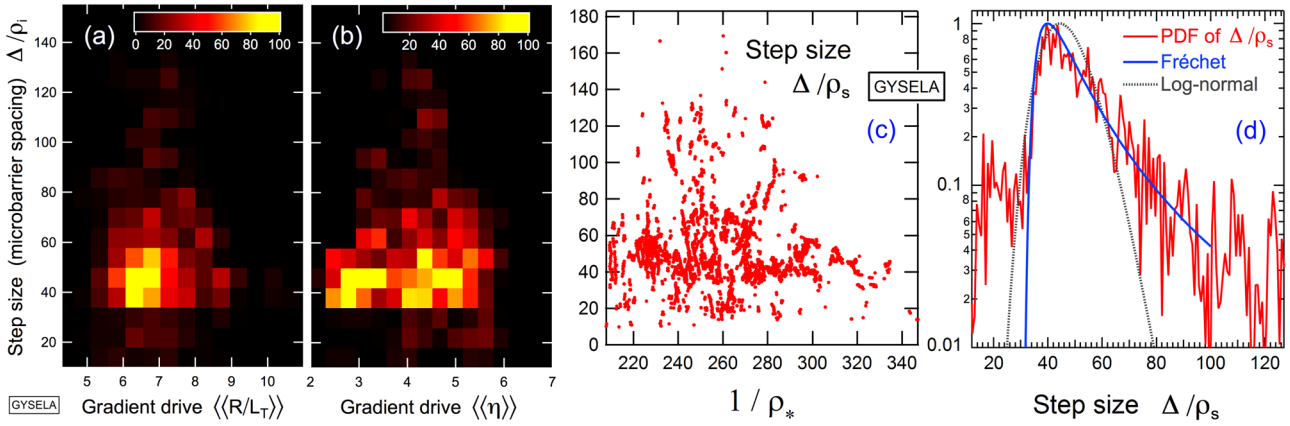

Figure 17. Staircase microbarrier spacing Δ normalised to the local ion Larmor radius as a function (*a*) and (*b*) of gradient drive (distance to marginality) and of (*c*) plasma size $\rho_\star^{-1}$. The statistics of step sizes Δ is shown in (*d*). The most probable microbarrier spacing is $\Delta^{\rm stat} = 40 \pm 2\,\rho_s$. Δ however can be large, displaying statistics of heavy-tailed distributions: a Fréchet distribution approximates it well, which is symptomatic of extreme value statistics.

- degraded confinement: favoured in the case of weak or vanishing microbarriers or when avalanching dominates across a large portion of the plasma.

To investigate the relative strength of microbarriers and avalanches, microbarrier shear strength equation (2) (as a measure of microbarrier permeability [21]) is a useful quantity—see section 2.2. From the above section 2.4.1 however, statistics of the step size of the staircase Δ is possibly a more robust observable of microbarrier permeability. Avalanches indeed do not cross staircase microbarriers without perturbing them and possibly destroying them, either way leaving a footprint on Δ. Δ *is thus a measure of the least favourable radial transport scale length in the system*: larger values are indicative of degraded confinement and its systematic computation conveys information on the actual transport processes.

Gyro-Bohm scaling through successive staircase steps. As in figure 12, since $r_{\rm step}(L_T, L_n)$ is a function of temperature and density gradients, Δ can be displayed as a function of ambient gradient drive as well as of $\rho_\star$. Its statistics are shown in figure 17. The colourscale in subplots (*a*) and (*b*) represent how often a given binned Δ value is found (the most encountered value is normalised to 100) as a function of ambient drive. Subplot (*c*) displays its behaviour with respect to $\rho_\star$. The larger Δ values correspond to temporary destruction of staircase steps, often prior to their reconstruction elsewhere. As compared to our earlier results [1, 20], the present dataset is larger, encompassing steady-state weakly driven plasmas (mostly using thermal bath boundary conditions) as well as more strongly driven (hence less quiescent) plasmas. The rich dynamics of the staircase pattern is now also embedded in the dataset, hence a large distribution of step sizes visible in subplot (*d*) and a slightly larger most probable step size $\Delta^{\rm stat} = 40 \pm 2\,\rho_s$ (the uncertainty reflects a 95% confidence interval). The most probable staircase step spacing also appears quite independent of the ambient drive—subplots (*a*) and (*b*).

Interestingly, despite statistical variability, the $\Delta^{\rm stat}$ scale is approximately constant throughout the scanned $\rho_\star$ values. This fact is strongly suggestive of a *gyro-Bohm scaling for the heat transport*, reintroduced in the system *despite avalanching*, via the mesoscale and $\rho_\star$ independent $\Delta^{\rm stat} \sim 40\,\rho_s$ *scaling of the staircase step layers*. In this regime of parameters (near-marginal, low-collisional), heat transport tends to a gyro-Bohm scaling owing to the successive staircase steps. We note also that the physics of why a gyro-Bohm scaling may here be found, statistically, is significantly different from diffusive/random walk arguments of turbulent transport scaling with the local microscale $\ell_c \sim 6\rho_s$ (see figure 3).

Extreme deviations, physical interpretation. A well defined scale $\Delta^{\rm stat}$ is observed with yet significant deviations from it. The distribution of step sizes in figure 17(*d*) is characteristic of fat-tailed distributions and is well described by a Fréchet distribution, a special case of Weibull (or generalized extreme value) distributions with lower bound:

$$\mathcal{F}(\Delta) = \frac{\tau^{1+\kappa}}{\sigma}\,\mathrm{e}^{-\tau} \quad \text{with } \tau = \left(1 + \kappa\frac{\Delta-\mu}{\sigma}\right)^{-1/\kappa} \qquad (3)$$

with respectively a scale parameter $\sigma = 10$, a location $\mu = 44$ and a shape $\kappa = 0.6$. As also shown in figure 17(*d*) a log-normal distribution, obtained through the multiplicative product of many independent random positive variables decays too fast and inaccurately describes the right tail of steps sizes. Fréchet PDF tails naturally emerge from the products of a finite number of random correlated variables and is often used as a phenomenological description of relaxation in disordered systems [52].

The observation of Fréchet statistics illustrates interesting aspects of the physics of staircase organisation. Fréchet (or Weibull) statistics naturally arise in the description of wear and tear of a system that is said to fail when either wear and tear accumulates beyond an acceptable level or if a fatal shock occurs. If the occurrences of fatal shocks can be modeled by a Poisson process whose rate function is state-dependent and if a random process governs the system state, then wear and tear statistics are often well described by Weibull distributions.

In analogy, if we postulate that the PDF of staircase step spacing emerges from disruptions of individual staircase steps, it is possible to connect the global statistics of Δ to the statistics of 'wear and tear' of individual steps. The state of individual steps results from a random process: the organisation of turbulence. Through avalanching, a natural state-dependent disruptive process continuously happens within the system, the size distribution of avalanches closely obeying Poisson statistics. In such framework, Fréchet statistics for staircase step spacing naturally emerges through combined influence of *both* the turbulent generation of staircase steps and the disruptive termination by avalanches.

Comparable statistics would certainly be observed if avalanches were to be understood not only as responsible for traumatic disruptions of individual staircase steps but also as *active participants in the onset of individual shear layers*. In the latter interpretation, both the life-time *and* the birth-rate [17] of staircase shear layers is influenced by avalanches and similar Fréchet statistics for Δ would certainly be expected. Either way, the observation of a Fréchet distribution equation (3) would then stand for a signature of avalanches in the global organisation of near-marginal plasma turbulence.

Lastly, it could be argued that a power law description could also fit the data in figure 17(*d*) rather than a stretched exponential [53]. A power law would characterise an absence of characteristic size for staircase step spacing. Clearly self-similarity at all scales is not observed but self-similarity could be argued beyond $\Delta^{\mathrm{stat}} \sim 40\,\rho_s$ as it is known that when accounting for finite size effects in a dataset a power law often crosses over to an exponential decay, hence leading to the curvature in the log-log plot observed in figure 17(*d*). However, with the Fréchet interpretation above, there is little need to invoke finite size effects to explain the fact that Δ statistics deviates from a power law.

What does it suggest for transport scaling? Both observations above suggest a route as to how a system described by strongly *non-Gaussian statistics* may display *favourable gyro-Bohm like transport* provided, as the system increases in size, that enough staircase microbarriers are formed. In addition to microscale regulation via shear suppression [54–56], transport can thus be *directly regulated at mesoscales* via modulation of front propagation at the *scale of the staircase step width*.

Figure 13 predicts an unfavourable scaling of staircase microbarrier strength with decreasing $\rho_\star$. Recent experimental findings (see figure 3 in [21]) tend to display a comparable trend. No such behaviour is visible in figure 17(*c*). Further understanding the statistics of Δ with decreasing $\rho_\star$ is certainly a matter of importance to understand the $\rho_\star$ scaling of heat transport. Improved confinement may reside in accessing regimes with faster decaying tails for the Δ (avalanche) distribution, provided the staircase structure survives. An unfavourable behaviour of the tail of the avalanche distribution on the other hand may provide a natural route to gyro-Bohm breaking.

3. Robustness of staircase microbarriers...

We focus the discussion on the robustness of organised staircase patterns with varying plasma parameters.

3.1. ...with respect to low-order q rationals

Localisation of spontaneous microbarriers for transport (i.e. the staircase steps) is an important question. In the case of developed so-called internal transport Barriers (ITBs), the connection with low-order rational values of the safety factor as well as with the shape of its profile has been previously emphasised both experimentally and in early modeling attempts [57, 58]. ITBs have been analysed to nucleate next to low-order rational q surfaces, especially at negative or vanishing magnetic shear. Linearly indeed, turbulent modes tend to resonate on distinct $q = m/n$ surfaces, their local growth rates being influenced both by the value of q and of its gradient. Two arguments are usually invoked for internal transport barrier onset: (i) low wavenumber turbulence tends to generate a localised $\mathbf{E} \times \mathbf{B}$ shear flow in the vicinity of low-order rational q surfaces or (ii) low wavenumber resonant surfaces tend to rarefy in reversed shear plasmas in the vicinity of vanishing magnetic shear, favouring the onset of $\mathbf{E} \times \mathbf{B}$ shear flows and the triggering of a barrier.

We test both ideas, asking:

- may staircase microbarriers form under similar influence of low-order q rationals?
- may the dynamic evolution of staircase steps lead to the formation of macroscopic ITBs, and if so is it in connection with the shape of the q profile?

To this end different situations are tested where the safety factor profile is varied: either parabolic and monotonically increasing—different cases are shown in figures 18 through 21—or reversed as also shown in figure 21, the location of vanishing magnetic shear corresponding to the low-order $q = 3/2$ rational. Anticipating on the results, the answer so far to both questions above is negative, yet might be worth considering anew with future inclusion of passing electron dynamics [27].

As previously shown [20, 21], neither the birth location of the staircase steps, nor their statistical localisation during nonlinear evolution seems to display clear correlations with low-order safety factor q rationals, in either monotonic or reversed q profiles. This is shown for the monotonic case in figures 18 and 19, with the possible exception of the $q = 2$ rational surface. Figure 20 records how often in the temporal window $t \in [500, 3900]\, a/c_s$ staircase microbarriers are found in the vicinity of given q values. From it, $q = 2$ could be defined as a 'sticky' location: staircase steps are not borne at this location but seem either attracted or prone to lingering in its vicinity. However, it is never the same staircase step but rather successive steps that linger near to $q = 2$ nor does this behaviour lead to the formation of a macroscopic ITB. This behaviour may be reminiscent of some experimental observations—e.g. shown next to the

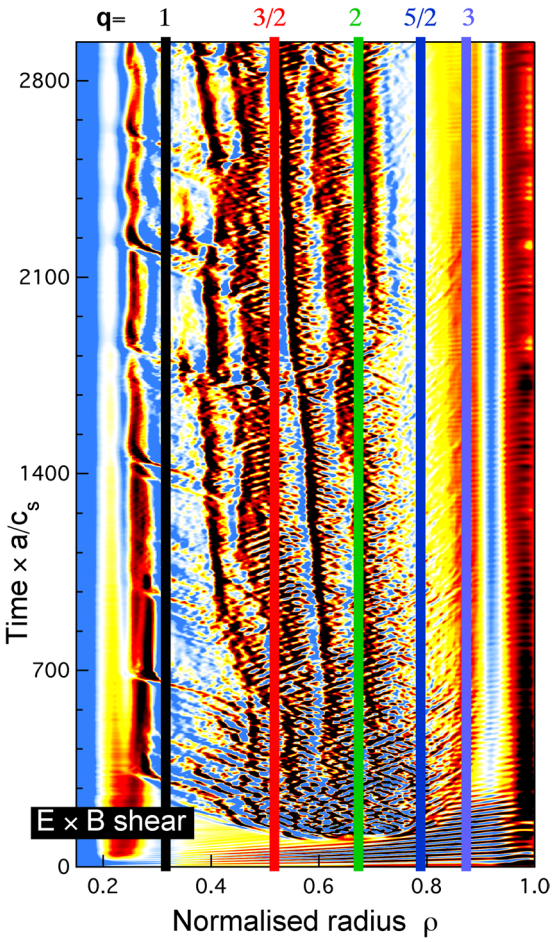

Figure 18. Same data as in figure 2 where the fixed locations of low-order $q = 1,\ 3/2,\ 2,\ 5/2$ and 3 rationals are superimposed on top of the $\mathbf{E} \times \mathbf{B}$ shear, marking the staircase steps. No clear connection between low-order q rationals and staircase microbarriers can be inferred.

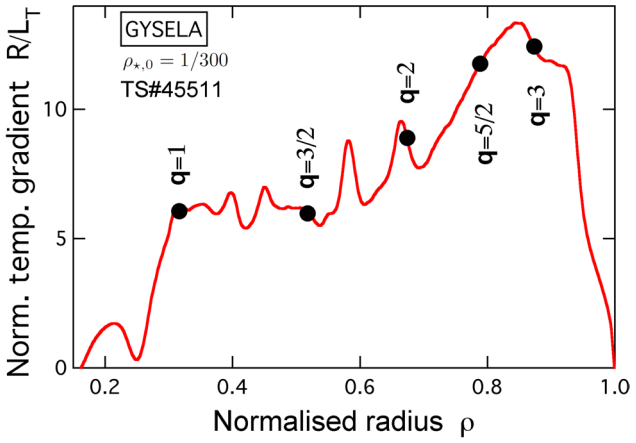

Figure 19. Gradient drive from figure 18 averaged between 2100 and 2892 a/c_s.

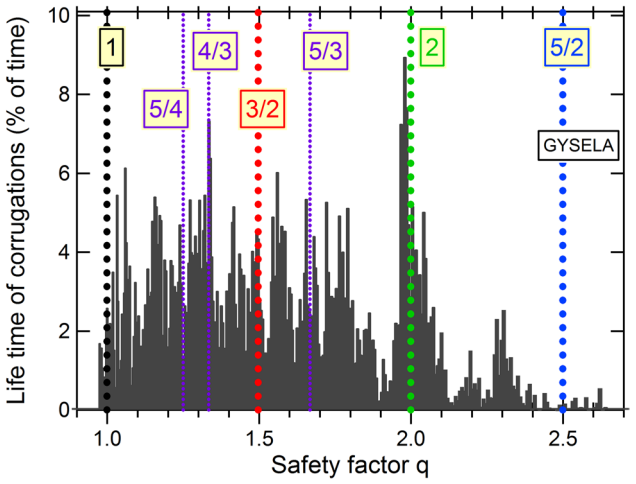

Figure 20. Statistics from figure 18 of the time staircase microbarriers (tracked as temperature corrugations) have spent in the vicinity of given q values, between $t = 500$ and $3900\, a/c_s$.

$q = 5/2$ surface (labelled S_0) in figure 3 of [20]—where measured wells in the radial correlation of turbulent fluctuations (interpreted as staircase microbarriers) are especially marked only when they coincide with a low-order q rational.

No other low-order rational in figure 20 however seems to display a similar behaviour than $q = 2$: the lifetime of temperature corrugations (i.e. microbarrier localisation) with respect to q locations is roughly evenly distributed. Possible synergies might thus exist between low-order q rationals and staircase microbarriers during their dynamic evolution but they seem rather weak. This observation may alert to the dubiety of quasilinear frameworks to correctly address staircase onset and dynamics.

A monotonically increasing q profile is now compared to a reversed q profile in figure 21, other parameters kept identical. At mid radius $\rho = 0.5$ the two profiles cross the $q = 3/2$ surface. This surface plays no noticeable role in the monotonically increasing q case. In the reversed shear case the central staircase step only, close to the minimum $q = 3/2$ location appears to be weakly drawn to this location. Furthermore, a limited steepening of the temperature gradient around the q reversal location is observed, visible through lower R/L_T values before $\rho = 0.5$ and larger ones afterwards. Both effects however are modest: (i) the staircase step does not rigorously locate at the minimum q location and even remains in the positive magnetic shear region during the computed evolution and (ii) the negative or vanishing magnetic shear does not lead to the formation of a macroscopic ITB either through an increased flow-gradient feedback or through coalescence of staircase microbarriers. Main conclusions are:

- the birth of staircase microbarriers is not correlated to low-order q rationals;
- correlation between staircase microbarriers and q rationals remains modest during nonlinear evolution despite observation of weak synergies;
- these synergies have not been observed to lead to staircase microbarrier coalescence or macroscopic ITB onset, even at low or reversed magnetic shear.

3.2. ...in time: staircase dynamics and meandering

The $\mathbf{E} \times \mathbf{B}$ staircase undergoes dynamic evolution (i) on the short timescale of avalanche emission as propagating

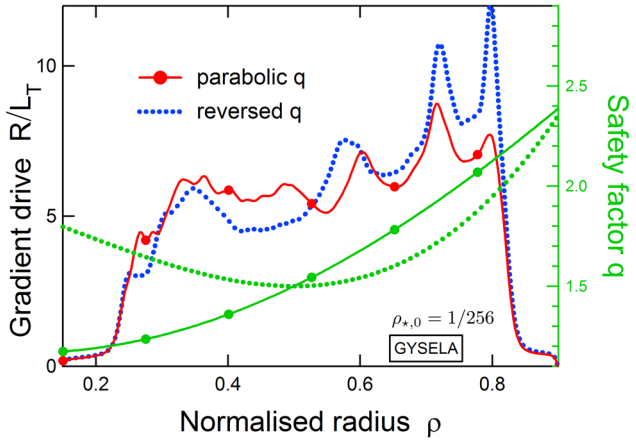

Figure 21. Same data as in figure 5, averaged between 4000 and 4610 a/c_s. Two situations are compared: all other parameters being equal, the safety factor profile is either parabolic or reversed. A weak response of the central staircase step to the reversed magnetic shear is observed.

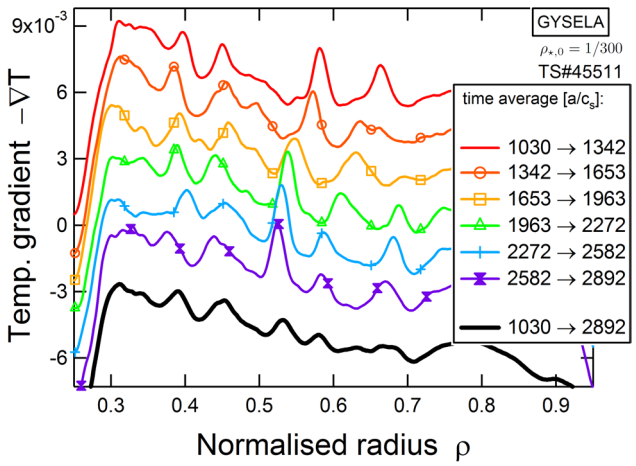

Figure 22. How the meandering of the $\mathbf{E} \times \mathbf{B}$ staircase leads to its seeming disappearance when time integration is large. Radial coarse-graining leads to the same result. This sets constrains on experimental time and space resolution in order to resolve the staircase structure. For clarity, the curves at different times have been vertically offset from each other.

avalanches interact with its microbarriers. This point has been evoked in the previous section and is emphasised through observation in figure 17(d) of Fréchet (Weibull) statistics for the staircase step size. Staircase steps may then drift radially or be destroyed by rare and large-scale avalanches impinging on them but usually reform in their wake, possibly at different radial locations. This short timescale for local staircase dynamics depends on distance to marginality (figure 4): close as well as far above marginality, the staircase pattern is less robust and easily perturbed by front dynamics.

Corrugations also evolve (ii) on the longer timescale of mean profile (and hence gradient drive) evolution as it adapts to the heat source. Corrugations display a slow radial motion that roughly tracks the ambient gradient drive $\langle\langle R/L_T \rangle\rangle$ evolution (see definition above, section 1.1). The radial locations of the staircase shear layers seem to remain at constant $\langle\langle R/L_T \rangle\rangle$ values. This propensity of corrugations to remain at constant ambient gradient drive [20, 21] is referred to as 'meandering'. Corrugations may endure from milliseconds to tens of milliseconds (the current upper limit of large-scale flux-driven computations). Their meandering timescale however is usually shorter, as illustrated in figure 22. The gradient is computed through sliding profile averages of $\sim$312 a/c_s that roughly correspond to $\sim$0.89 ms starting at time 1030 a/c_s. For visualisation purposes, a negative offset of 0.002 is applied to each time-slice. Clearly the staircase pattern exists throughout the time slice displayed here yet a global averaging between 1030 and 2892 a/c_s would effectively smear it out.

Experimentally, staircase steps are tracked as local minima of the coherence length profile $\langle L_{\rm coh} \rangle_{\rm F}$ of density fluctuations, the procedure as described in [20, 21]. The meandering of the $\langle L_{\rm coh} \rangle_{\rm F}$ wells is uneasy to characterise and seems to occur on long time scales. An example is shown in figure 23. Displacement of the $\langle L_{\rm coh} \rangle_{\rm F}$ profile, not detectable during a single acquisition (6 ms) becomes more visible when comparing successive acquisitions separated by 5 to 10 s. The

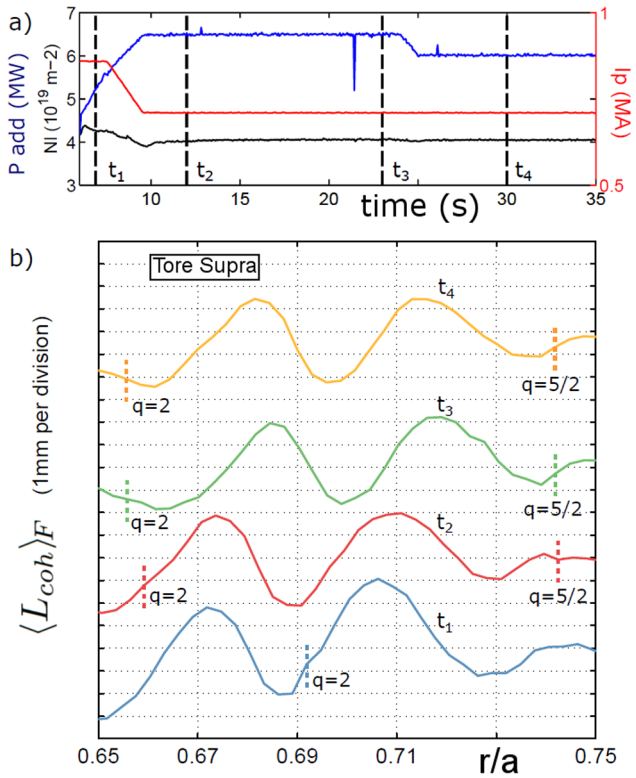

Figure 23. Experimental coherence length profiles $\langle L_{\rm coh} \rangle_{\rm F}$ of density fluctuations at times t_1 through t_4.

present data cannot allow to unambiguously determine whether the similarity of the coherence length waveforms measured during the successive acquisitions in figure 23 results from a single very long-lived staircase or rather from staircase patterns that have repeatedly disappeared and reformed. The disparity of time scales observed in experiments and simulations is yet a challenge to explain.

4. Conclusions and outlook

The $\mathbf{E}\times\mathbf{B}$ staircase of magnetised plasmas is a spontaneous global-scale organisation of localised microbarriers for transport interspersed between regions of turbulent avalanching. Microbarriers coincide with long-lived corrugations of the mean plasma profiles. The $\mathbf{E}\times\mathbf{B}$ staircase pattern spontaneously arises in near-marginal (section 1.1) and low-collisional (section 1.2) regimes, emphasising its possible relevance for forthcoming large-scale fusion experiments. The staircase pattern is a nonlinear feature of turbulence self-organisation. Linear properties of the system do not appear to play a visible role for its localisation, slow dynamics or fast reorganisation (sections 3.1 and 3.2).

Staircase organisation expresses a modification in the nature rather than in the overall magnitude of zonal flow shear as incoherent zonal disturbance flows (dominant in gradient-driven approaches) coalesce into temporally coherent and spatially concentrated zonal mean flows (dominant in flux-driven approaches) (sections 2.1 and 2.2). Positive feedback between zonal mean flows and mean plasma gradients is dynamically important to $\mathbf{E}\times\mathbf{B}$ staircase onset (section 2.2).

The space-time coherence of zonal mean shear at the staircase steps (possible through the positive feedback on the mean gradients) impacts heat transport levels globally (section 2.3). For a given level of zonal flow activity, staircase organisation results in better confinement than when absent, its successive shear layers being active barriers for transport. The flux-gradient relation is notably modified at the onset of staircase patterning: it becomes intrinsically multivalued, non-monotonic (regions of staircase existence can display a negative diffusion type of behaviour: heat accumulation with increasing gradient) and evolves dynamically. A consequence is that local fluxes may not be unambiguously estimated merely based on the knowledge of local profile values L_T or L_n, in stark contrast with the rationale behind gradient-driven approaches.

As zonal mean flows concentrate spatially in the narrow regions of the staircase microbarriers, avalanche-type of events fill the space in-between microbarriers. These layers, of typical radial extent $\delta^{\mathrm{flow}}\sim 10\rho_s$ efficiently contribute to contain the avalanche-like transport (section 2.4.1). As the most probable staircase step spacing $\Delta^{\mathrm{stat}}\sim 40\,\rho_s$ is mesoscale (the spacing between adjacent microbarriers), avalanching is also statistically contained to mesoscales. Despite avalanching and non-Gaussian transport statistics a favourable gyro-Bohm like scaling for transport is found provided that enough successive staircase shear layers are formed (section 2.4.2).

It is worth noticing that the rationale here for gyro-Bohm scaling is based upon mesoscale Δ^{stat} balance between avalanches and staircase microbarriers. The physical picture is thus significantly different than diffusion or random walk at the scale of local turbulence autocorrelation length $\ell_c\propto\rho_s$. This fact also suggests that in addition to the classical microscale regulation via shear suppression, transport can be directly regulated at mesoscales via modulation of front propagation at the scale of the staircase step width (section 2.4.2).

This dynamic interplay between avalanches and microbarriers, two natural trends of the near-marginal plasma opens a natural route to understand the physics of either gyro-Bohm scaling or of gyro-Bohm breaking, in a unified framework. Given which one of (beneficial) staircase microbarriers or (detrimental) avalanches dominates may help explaining gyro-Bohm breaking situations (avalanching dominant), gyro-Bohm scaling (mesoscale spaced microbarriers) or possibly improved confinement (microbarriers become impermeable or coalesce).

In this perspective the scaling of microbarrier shear strength σ_{step} (a measure of microbarrier permeability) or of step spacing Δ with system size $\rho_\star^{-1}$ may be key to understand the scaling of transport with $\rho_\star^{-1}$ [21]. The trend with $\rho_\star^{-1}$ for microbarrier shear strength seems unfavourable (section 2.2) whilst the trend for step spacing is favourable with the emergence of scale Δ^{stat} (section 2.4.2). An important question for transport scaling as $\rho_\star^{-1}$ increases towards ITER values is that of the trade-off between this possibly unfavourable microbarrier weakening and the beneficial increase in the number of staircase steps.

Some concluding remarks:

(a) Relatively new in magnetised plasma turbulence, staircases are however commonly observed in many geo- or astrophysical systems. The interested reader for non-magnetised plasma systems is referred (non exhaustively) to [11, 12, 59–62];

(b) Turbulence regulation within the staircasing plasma depends dominantly on zonal mean shear patterning. This fact accredits the idea already in [63] of a system better described by one prey (the turbulence), two predators (zonal disturbance and zonal mean flows), with one predator (the mean flow) also preying on the other (the disturbance flow) flow). The added fact is that the system *globally organises staircase-wise*;

(c) Staircases are identified in actual plasmas [20, 21] through observation of their successive shear layers, so far in ion drift-wave turbulence regimes using correlation analysis of *density fluctuations* from ultrafast-sweeping reflectometer data. When turbulence results from a mixture of free energy sources (ion and electron drift-wave) as is the case at the transition between saturated ohmic confinement (SOC) and linear ohmic confinement (LOC), staircase signatures seem more complex to identify [21]. Correlation analysis performed as in above references but based upon high-resolution *electron temperature fluctuations* would appear as an important step to further assess the generic character of staircase organisation for drift-wave turbulence.

Acknowledgments

The authors want to thank Ch. Passeron for continued help with the development of GYSELA, Y. Asahi, F. Clairet, E. Caschera, P.H. Diamond, P. Donnel, Ö.D. Gürcan, D.W. Hughes, Y. Idomura, Y. Kosuga, A. Milovanov and the participants at the Festival de Théorie, Aix-en-Provence and at the

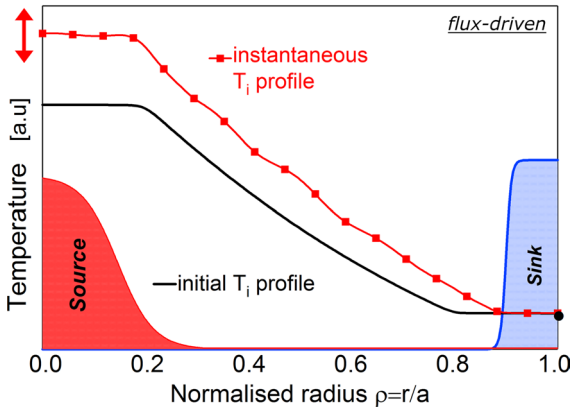

Figure A1. Typical heat flux-driven setup.

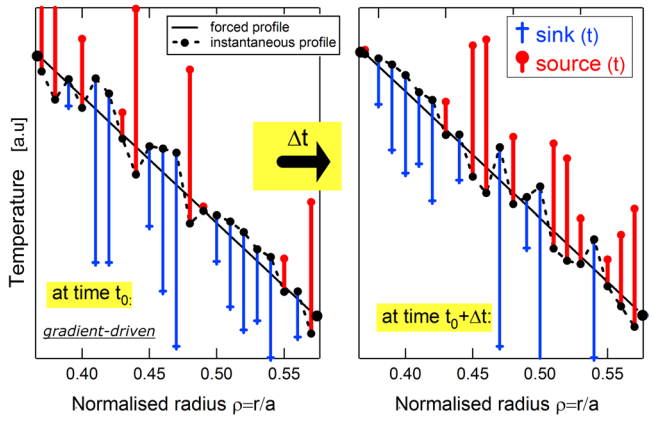

Figure A2. Evolution, as the temperature fluctuates, of the adaptive gradient-driven source/sink equation (A.2) from one time step t_0 to a next $t_0 + \Delta t$. The gradient-driven forced profile (solid line) is computed from the flux-driven mean $T_{\text{F-D}}$ profile in figure 24 and coincides with the flux-driven 'ambient mean profile', as defined on page 3. For clarity, only a zoom between $\rho = 0.37$ and 0.57 is shown.

Kavli Institute for Theoretical Physics, Santa Barbara. GDP acknowledges support from the Guest Professor Programme from the University of Tokyo. This work has been carried out within the framework of the French Research Federation for Fusion Studies and of the EUROfusion Consortium and has received funding from the Euratom research and training programme 2014-2018 under grant agreement No 633053 for the projects WP14-ER-01/IPP-02 and WP17-ER/ENEA-10. The views and opinions expressed herein do not necessarily reflect those of the European Commission. This research was supported in part by the National Science Foundation under Grant No. NSF PHY-1125915. We benefited from HPC resources from GENCI, CCRT-TGCC and IFERC.

This work is dedicated to the memory of Steve Jaeger, untimely deceased.

Appendix A. Same code, two frameworks: flux- versus gradient-driven forcing

The usual flux-gradient paradigm [26] relates local values for heat fluxes to local values of the gradients η—or R/L_T in the case of ITG with low to moderate L_n, *with fixed mean values for the turbulence drive, i.e. fixed mean profiles.* This approach is referred to as 'fixed-gradient' or 'gradient-driven' (G-D) as opposed to 'flux-driven' (F-D) where both fluxes and profiles evolve consistently [64] and are unknown functions of the dynamics. Formally, the flux-driven gyrokinetic equation solved in GYSELA reads:

$$\frac{\mathrm{D}f}{\mathrm{D}t} \equiv \frac{\partial f}{\partial t} - [H, f] = \mathcal{C}(f) + \mathcal{S}(f) \qquad \text{(A.1)}$$

where f represents the full ion distribution function, H the gyrokinetic Hamiltonian [65], $\mathcal{C}$ the collision operator [36, 37] and $\mathcal{S}$ the source [7]. The flux-driven computations throughout the paper are heat-driven only and a typical example is shown in figure A1.

Switching between a flux- and a gradient-driven framework is done whilst replacing the source term in equation (A.1) by a Krook-type operator that acts as both a source or a sink, depending on the dynamics (the sign of $f - \mathbb{F}_{\text{F-D}}$) and driving a restoring force with strength γ^{K} towards the chosen mean profiles $\mathbb{F}_{\text{F-D}}$:

$$\frac{\mathrm{D}f}{\mathrm{D}t} = \mathcal{C}(f) - \gamma^{\text{K}}\left[f - \mathbb{F}_{\text{F-D}}\left(1 + \frac{\langle f - \mathbb{F}_{\text{F-D}}\rangle}{\langle \mathbb{F}_{\text{F-D}}\rangle}\right)\right] \qquad \text{(A.2)}$$

with $\langle\cdot\rangle = \int \mathrm{d}\mathbf{v}\mathrm{d}\theta\mathrm{d}\varphi\, \mathcal{J}_v\mathcal{J}\,\cdot$, $\mathcal{J}_v$ and $\mathcal{J}$ being the velocity and space Jacobians. The adaptive dynamics of the source/sink equation (A.2) is shown in figure A2. The last term in equation (A.2) is usual prescription for gradient-driven models [66] so as to prevent overdamping the zonal modes.

In practice, in order to compare flux- and gradient-driven approaches, the target distribution $\mathbb{F}_{\text{F-D}}$ in equation (A.2) is constructed from a steady flux-driven distribution function. The following procedure is applied that allows GYSELA to mimic usual computations at fixed gradient:

(i) a flux-driven computation is run until flux equilibrium. Mean density $n_{\text{F-D}}$, temperature $T_{\text{F-D}}$ and flow profiles are computed;
(ii) corrugations are removed from the above flux-driven mean profiles resulting in smooth equivalent mean profiles;
(iii) an equivalent Maxwellian distribution $\mathbb{F}_{\text{F-D}}$ is built from these smooth profiles and imposed in equation (A.2);
(iv) linear stability is computed for the base state $\mathbb{F}_{\text{F-D}}$. Unusable global modes grow with a maximum growth rate γ_{lin};
(v) the 'spring constant' γ^{K} in equation (A.2) is chosen such that it has no notable effect on the linear instability growth of the ITG *and* nonlinearly such that the root mean square (RMS) of the electric potential fluctuations $(\delta\Phi^2)^{1/2}$, a measure of the turbulence intensity is comparable in both flux-driven and gradient-driven approaches. This is shown in figure A3. γ^{K} has been varied between $\gamma_{\text{lin}}/3$ and $\gamma_{\text{lin}}/15$. The results in the paper are qualitatively

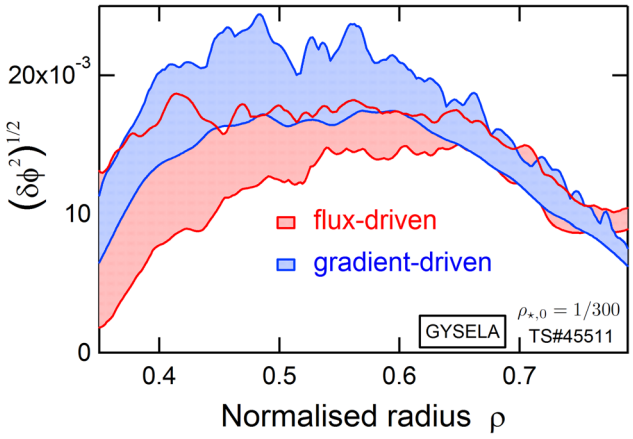

Figure A3. The 'spring constant' γ^K in equation (A.2) (here $\gamma^K = 5.43\,10^{-5}\,\omega_{c,i} = \gamma_{lin}/10$) is chosen such that it agrees with usual prescriptions for gradient-driven models $\gamma^K \sim \gamma_{lin}/10$. With this prescription, computed turbulence intensities $(\delta\Phi^2)^{1/2}$ with GYSELA in flux- and gradient-driven approaches agree within 15–20%.

independent of the precise choice of γ^K. Unless otherwise stated: $\gamma^K = \gamma_{lin}/10$, consistently with [66];

(vi) the gradient-driven calculation is compared to the reference flux-driven computation at quasi steady-state for the flows and the fluctuations.

Through this procedure, flux- and gradient-driven computations have near-identical ambient mean gradients, as defined in section 1.1.

Note that the gradient-driven approach of equation (A.2) contains additional physics as compared to usual gradient-driven approaches. In the latter a scale separation is usually performed in the equations so that formally the total $f = F_0 + \delta f$ and $H = H_0 + \delta h$ are divided into a background distribution F_0 and equilibrium Hamiltonian H_0, fixed in time and fluctuating parts δf and δh. The mean evolution $\partial_t F_0$ is discarded and so are nonlinear advection terms that contribute to its evolution, formally written $\langle[\delta h, \delta f]\rangle$, with $\langle\cdot\rangle$ representing an ensemble averaging. Only δf dynamically evolves and the consistency of the performed separation of scales $\delta f/F_0 = O(\epsilon)$ has to be checked throughout the computation. In GYSELA, the total f and H enter equation (A.1) and evolve so that the 'mean distribution' $\langle f\rangle$ (regardless of whether such a 'mean' is correctly approximated by an analytic (Maxwellian) F_0) tends to change and corrugate due to the turbulent dynamics—essentially due to the back-reaction of the small turbulence scales $\langle[\delta h, \delta f]\rangle$ on the larger, slower mean ones. Then the Krook-type operator is applied, partly restoring the mean profiles. The gradient-driven approach of GYSELA described by equation (A.2) thus contains features of turbulence self-organisation absent when a scale separation is performed. It is thus intermediate between flux-driven and more usual δf global gradient-driven approaches. Actual differences between F-D and δf G-D approaches, especially regarding structure formation are thus expected to be larger that the differences reported below.

Appendix B. How generic are the results comparing flux- and gradient-driven computations?

As expected, the discrepancies highlighted above between flux-driven and gradient-driven systems regarding pattern formation, shear flow generation and transport levels decrease with decreasing strength of γ^K in equation (A.2) and tend to (transiently) vanish in the limit $\gamma^K \to 0$. Mean profile corrugations, mean shear patterns, more coherent avalanche-type events and staircase organisation tend to appear in gradient-driven systems, as transients, at very low values of the restoring force e.g. $\gamma^K \sim \gamma_{lin}/100$. However at such low values of γ^K the mean profiles relax and turbulence decays as its drive is no longer sustained. This remark however tends to emphasise $\mathbf{E} \times \mathbf{B}$ staircase organisation as a natural tendency for the self-organising core plasma.

It is also worth noticing that both decaying turbulence computations as well as computations run with thermal baths at both radial boundaries (this represents a cruder and earlier version of the heat flux-driven computations shown in the paper and illustrated in figure A1, as the amount of heat actually injected in the system is not controlled) also exhibit staircase organisation, though transiently in the decaying case. The robustness of this form of organisation with respect to forcing also tends to emphasise staircase-avalanche interplay as a natural tendency for such systems, as soon as consistent feedback between flows, shear and mean profiles is allowed.

References

[1] Dif-Pradalier G., Diamond P.H., Grandgirard V., Sarazin Y., Abiteboul J., Garbet X., Ghendrih Ph., Strugarek A., Ku S. and Chang C.S. 2010 On the validity of the local diffusive paradigm in turbulent plasma transport *Phys. Rev.* E **82** 025401

[2] Diamond P.H. and Hahm T.S. 1995 On the dynamics of turbulent transport near marginal stability *Phys. Plasmas* **2** 3640–9

[3] Hwa T. and Kardar M. 1992 Avalanches, hydrodynamics, and discharge events in models of sandpiles *Phys. Rev.* A **45** 7002–23

[4] Carreras B.A., Newman D., Lynch V.E. and Diamond P.H. 1996 A model realization of self-organized criticality for plasma confinement *Phys. Plasmas* **3** 2903–11

[5] Newman D.E., Carreras B.A., Diamond P.H. and Hahm T.S. 1996 The dynamics of marginality and self-organized criticality as a paradigm for turbulent transport *Phys. Plasmas* **3** 1858–66

[6] Sarazin Y. and Ghendrih Ph. 1998 Intermittent particle transport in two-dimensional edge turbulence *Phys. Plasmas* **5** 4214–28

[7] Sarazin Y., Grandgirard V., Abiteboul J., Allfrey S., Garbet X., Ghendrih Ph., Latu G., Strugarek A. and Dif-Pradalier G. 2010 Large scale dynamics in flux driven gyrokinetic turbulence *Nucl. Fusion* **50** 054004

[8] Van Compernolle B., Morales G.J., Maggs J.E. and Sydora R.D. 2015 Laboratory study of avalanches in magnetized plasmas *Phys. Rev.* E **91** 031102

[9] Rosenbluth M.N. and Hinton F.L. 1998 Poloidal flow driven by ion-temperature-gradient turbulence in tokamaks *Phys. Rev. Lett.* **80** 724–7

[10] Diamond P.H., Itoh S.-I., Itoh K. and Hahm T.S. 2005 Zonal flows in plasma—a review *Plasma Phys. Control. Fusion* **47** R35–161

[11] Phillips O.M. 1972 Turbulence in a strongly stratified fluid—is it unstable? *Deep Sea Res. Oceanographic Abstr.* **19** 79–81

[12] Balmforth N.J., Smith S.G.L. and Young W.R. 1998 Dynamics of interfaces and layers in a stratified turbulent fluid *J. Fluid Mech.* **355** 329–58

[13] Hinton F.L. 1991 Thermal confinement bifurcation and the l-to h-mode transition in tokamaks *Phys. Fluids* B **3** 696–704

[14] Ashourvan A. and Diamond P.H. 2016 How mesoscopic staircases condense to macroscopic barriers in confined plasma turbulence *Phys. Rev.* E **94** 051202

[15] Flynn M.R., Kasimov A.R., Nave J.-C., Rosales R.R. and Seibold B. 2009 Self-sustained nonlinear waves in traffic flow *Phys. Rev.* E **79** 056113

[16] Kosuga Y., Diamond P.H. and Gürcan Ö.D. 2013 How the propagation of heat-flux modulations triggers $\mathbf{E}\times\mathbf{B}$ flow pattern formation *Phys. Rev. Lett.* **110** 105002

[17] Kosuga Y., Diamond P.H., Dif-Pradalier G. and Gürcan Ö.D. 2014 $\mathbf{E}\times\mathbf{B}$ shear pattern formation by radial propagation of heat flux wavesa *Phys. Plasmas* **21** 055701

[18] Itoh K. and Itoh S.-I. 2016 A structural bifurcation of transport in toroidal plasmas *Plasma Phys. Control. Fusion* **58** 045017

[19] Ghendrih P. *et al* 2014 Phase space structures in gyrokinetic simulations of fusion plasma turbulence *Eur. Phys. J.* D **68** 303

[20] Dif-Pradalier G. *et al* 2015 Finding the elusive $\mathbf{E}\times\mathbf{B}$ staircase in magnetized plasmas *Phys. Rev. Lett.* **114** 085004

[21] Hornung G., Dif-Pradalier G., Clairet F., Sarazin Y., Sabot R., Hennequin P. and Verdoolaege G. 2017 $\mathbf{E}\times\mathbf{B}$ staircases and barrier permeability in magnetised plasmas *Nucl. Fusion* **57** 014006

[22] Helander P. and Sigmar D.J. 2005 *Collisional Transport in Magnetized Plasmas* (Cambridge: Cambridge University Press)

[23] Dif-Pradalier G., Grandgirard V., Sarazin Y., Garbet X. and Ghendrih Ph. 2009 Interplay between gyrokinetic turbulence, flows, and collisions: Perspectives on transport and poloidal rotation *Phys. Rev. Lett.* **103** 065002

[24] Hinton F.L. and Rosenbluth M.N. 1999 Dynamics of axisymmetric $\mathbf{E}\times\mathbf{B}$ and poloidal flows in tokamaks *Plasma Phys. Control. Fusion* **41** A653–62

[25] Hennequin P. *et al* 2015 Comprehensive experimental study of plasma turbulence structure and its scaling with $\rho_\star$ *42nd EPS Conf. (Lisbon, Portugal, 22–26 June 2016)* (http://ocs.ciemat.es/EPS2015ABS/pdf/I1.102.pdf)

[26] Dimits A.M. *et al* 2000 Comparisons and physics basis of tokamak transport models and turbulence simulations *Phys. Plasmas* **7** 969–83

[27] Dominski J., Brunner S., Aghdam S.K., Grler T., Jenko F. and Told D. 2012 Identifying the role of non-adiabatic passing electrons in itg/tem microturbulence by comparing fully kinetic and hybrid electron simulations *J. Phys.: Conf. Ser.* **401** 012006

[28] Grandgirard V. *et al* 2007 Global full-f gyrokinetic simulations of plasma turbulence *Plasma Phys. Control. Fusion* **49** B173–82

[29] Grandgirard V. *et al* 2016 A 5d gyrokinetic full- global semi-lagrangian code for flux-driven ion turbulence simulations *Comput. Phys. Commun.* **207** 35–68

[30] Rath F., Peeters A.G., Buchholz R., Grosshauser S.R., Migliano P., Weikl A. and Strintzi D. 2016 Comparison of gradient and flux driven gyro-kinetic turbulent transport *Phys. Plasmas* **23** 052309

[31] Lin Z., Hahm T.S., Lee W.W., Tang W.M. and Diamond P.H. 1999 Effects of collisional zonal flow damping on turbulent transport *Phys. Rev. Lett.* **83** 3645

[32] Abiteboul J. *et al* 2013 Turbulent momentum transport in core tokamak plasmas and penetration of scrape-off layer flows *Plasma Phys. Control. Fusion* **55** 074001

[33] Idomura Y. and Nakata M. 2014 Plasma size and power scaling of ion temperature gradient driven turbulence *Phys. Plasmas* **21** 020706

[34] Norscini C. *et al* 2014 Turbulent transport close to marginal instability: role of the source driving the system out of equilibrium *J. Phys.: Conf. Ser.* **561** 012013

[35] Hinton F.L. and Hazeltine R.D. 1976 Theory of plasma transport in toroidal confinement systems *Rev. Mod. Phys.* **48** 239–308

[36] Dif-Pradalier G. *et al* 2011 Neoclassical physics in full distribution function gyrokinetics *Phys. Plasmas* **18** 062309

[37] Estève D., Garbet X., Sarazin Y., Grandgirard V., Cartier-Michaud T., Dif-Pradalier G., Ghendrih P., Latu G. and Norscini C. 2015 A multi-species collisional operator for full-f gyrokinetics *Phys. Plasmas* **22** 122506

[38] Nakata M. and Idomura Y. 2013 Plasma size and collisionality scaling of ion temperature gradient driven turbulence *Nucl. Fusion* **53** 113039

[39] Thom R. 1994 *Structural Stability and Morphogenesis* (Boulder, CO: Westview Press)

[40] Diamond P.H., Lebedev V.B., Newman D.E., Carreras B.A., Hahm T.S., Tang W.M., Rewoldt G. and Avinash K. 1997 Dynamics of transition to enhanced confinement in reversed magnetic shear discharges *Phys. Rev. Lett.* **78** 1472–5

[41] Garbet X., Mantica P., Ryter F., Cordey G., Imbeaux F., Sozzi C., Manini A., Asp E., Parail V., Wolf R. and The JET EFDA Contributors 2004 Profile stiffness and global confinement *Plasma Phys. Control. Fusion* **46** 1351

[42] Lin Z., Ethier S., Hahm T.S. and Tang W.M. 2002 Size scaling of turbulent transport in magnetically confined plasmas *Phys. Rev. Lett.* **88** 195004

[43] Scott B.D., Biglari H., Terry P.W. and Diamond P.H. 1991 Self-organization in sheared drift-wave turbulence *Phys. Fluids* B **3** 51–67

[44] Holland C. *et al* 2011 Advances in validating gyrokinetic turbulence models against l- and h-mode plasmas *Phys. Plasmas* **18** 056113

[45] Hahm T.S., Diamond P.H., Lin Z., Itoh K. and Itoh S.-I. 2004 Turbulence spreading into the linearly stable zone and transport scaling *Plasma Phys. Control. Fusion* **46** A323

[46] Dif-Pradalier G., Caschera E., Ghendrih Ph., Asahi Y., Donnel P., Garbet X., Grandgirard V., Latu G., Narscini C. and Sarazin Y. 2017 Evidence for global edge-core interplay in fusion plasmas *Plasma Fusion Res.* **12** 1203012

[47] Ghendrih Ph. *et al* 2012 Thermodynamical and microscopic properties of turbulent transport in the edge plasma *J. Phys.: Conf. Ser.* **401** 012007

[48] Idomura Y., Urano H., Aiba N. and Tokuda S. 2009 Study of ion turbulent transport and profile formations using global gyrokinetic full-f vlasov simulation *Nucl. Fusion* **49** 065029

[49] Mantica P. *et al* 2009 Experimental study of the ion critical-gradient length and stiffness level and the impact of rotation in the jet tokamak *Phys. Rev. Lett.* **102** 175002

[50] Sauter O. *et al* and TCV Team 2014 On the non-stiffness of edge transport in l-mode tokamak plasmas *Phys. Plasmas* **21** 055906

[51] Hillesheim J.C., Delabie E., Meyer H., Maggi C.F., Meneses L., Poli E. and JET Contributors 2016 Stationary zonal flows during the formation of the edge transport barrier in the jet tokamak *Phys. Rev. Lett.* **116** 065002

[52] Rinne H 2008 *The Weibull Distribution* (London: Chapman and Hall)
[53] Ghendrih Ph., Ciraolo G., Dif-Pradalier G., Norscini C., Sarazin Y., Abiteboul J., Cartier-Michaud T., Garbet X., Grandgirard V. and Strugarek A. 2014 Fusion plasma turbulence described by modified sandpile dynamics *Eur. Phys. J.* E **37**
[54] Biglari H.P., Diamond H. and Terry P.W. 1990 Influence of sheared poloidal rotation on edge turbulence *Phys. Plasmas* B **2** 1
[55] Waltz R.E. and Kerbel G.D. 1995 Advances in the simulation of toroidal gyro-landau fluid model turbulence *Phys. Plasmas* **2** 2408–16
[56] Hahm T.S. and Burrell K.H. 1996 $\mathbf{E} \times \mathbf{B}$ flow shear effects on radial correlation length of turbulence and gyroradius scaling of confinement *Phys. Plasmas* **3** 427–9
[57] Garbet X. *et al* and JET EFDA Contributors 2003 Micro-stability and transport modelling of internal transport barriers on jet *Nucl. Fusion* **43** 975
[58] Waltz R.E., Austin M.E., Burrell K.H. and Candy J. 2006 Gyrokinetic simulations of off-axis minimum-q profile corrugations *Phys. Plasmas* **13** 052301
[59] Merryfield W.J. 2000 Origin of thermohaline staircases *J. Phys. Oceanogr.* **30** 1046–68
[60] Dritschel D.G. and McIntyre M.E. 2008 Multiple jets as PV staircases: the phillips effect and the resilience of eddy-transport barriers *J. Atmos. Sci.* **65** 855–74
[61] Marcus P.S. and Shetty S. 2011 Jupiter's zonal winds: are they bands of homogenized potential vorticity organized as a monotonic staircase? *Phil. Trans. R. Soc.* A **369** 771–95
[62] Vallis G.K. 2006 *Atmospheric and Oceanic Fluid Dynamics* (Cambridge: Cambridge University Press)
[63] Kim E.J. and Diamond P.H. 2003 Zonal flows and transient dynamics of the L–H transition *Phys. Rev. Lett.* **90** 185006
[64] Garbet X., Sarazin Y., Beyer P., Ghendrih Ph., Waltz R.E., Ottaviani M. and Benkadda S. 1999 Flux driven turbulence in tokamaks *Nucl. Fusion* **39** 2063–8
[65] Garbet X., Idomura Y., Villard L. and Watanabe T.H. 2010 Gyrokinetic simulations of turbulent transport *Nucl. Fusion* **50** 043002
[66] McMillan B.F., Jolliet S., Tran T.M., Villard L., Bottino A. and Angelino P. 2008 Long global gyrokinetic simulations: source terms and particle noise control *Phys. Plasmas* **15** 052308